AFRL-OSR-VA-TR-2015-0190

Propellant-free Spacecraft Relative Maneuvering via Atmospheric Differential Drag

Kurt Anderson
RENSSELAER POLYTECHNIC INST TROY NY

07/06/2015
Final Report

DISTRIBUTION A: Distribution approved for public release.

Air Force Research Laboratory
AF Office Of Scientific Research (AFOSR)/ RTE
Arlington, Virginia 22203
Air Force Materiel Command

REPORT DOCUMENTATION PAGE

Form Approved
OMB No. 0704-0188

The public reporting burden for this collection of information is estimated to average 1 hour per response, including the time for reviewing instructions, searching existing data sources, gathering and maintaining the data needed, and completing and reviewing the collection of information. Send comments regarding this burden estimate or any other aspect of this collection of information, including suggestions for reducing the burden, to Department of Defense, Washington Headquarters Services, Directorate for Information Operations and Reports (0704-0188), 1215 Jefferson Davis Highway, Suite 1204, Arlington, VA 22202-4302. Respondents should be aware that notwithstanding any other provision of law, no person shall be subject to any penalty for failing to comply with a collection of information if it does not display a currently valid OMB control number.
PLEASE DO NOT RETURN YOUR FORM TO THE ABOVE ADDRESS.

1. REPORT DATE *(DD-MM-YYYY)*	2. REPORT TYPE	3. DATES COVERED *(From - To)*
06/10/2015	Final	15 April 2012 - 14 April 2015

4. TITLE AND SUBTITLE
(YIP) Propellant-free Spacecraft Relative Maneuvering via Atmospheric Differential Drag

5a. CONTRACT NUMBER

5b. GRANT NUMBER
FA9550-12-1-0072

5c. PROGRAM ELEMENT NUMBER

6. AUTHOR(S)
Kurt Anderson (Riccardo Bevilacqua)

5d. PROJECT NUMBER

5e. TASK NUMBER

5f. WORK UNIT NUMBER

7. PERFORMING ORGANIZATION NAME(S) AND ADDRESS(ES)
Rensselaer Polytechnic Institute

8. PERFORMING ORGANIZATION REPORT NUMBER

9. SPONSORING/MONITORING AGENCY NAME(S) AND ADDRESS(ES)
Air Force Office of Scientific Research - Space Propulsion and Power Program

10. SPONSOR/MONITOR'S ACRONYM(S)
AFOSR

11. SPONSOR/MONITOR'S REPORT NUMBER(S)

12. DISTRIBUTION/AVAILABILITY STATEMENT
DISTRIBUTION A

13. SUPPLEMENTARY NOTES

14. ABSTRACT
At low Earth orbits (LEO), a differential in the drag acceleration between spacecraft can be used to control their relative motion. This differential allows for a propellant-free method for performing relative maneuvers, which can reduce the costs of spacecraft formations. In this project atmospheric differential drag (DD) based nonlinear controllers are presented that can be used for planar relative maneuvers of two spacecraft. Furthermore, the atmospheric density varies in time and in space as the spacecraft travel along their orbits. In this project a localized density predictor based on Neural Networks is created and tested in its forecasting potential.

15. SUBJECT TERMS
Differential drag; Propellant-Free maneuvering; Nonlinear control

16. SECURITY CLASSIFICATION OF:			17. LIMITATION OF ABSTRACT	18. NUMBER OF PAGES	19a. NAME OF RESPONSIBLE PERSON
a. REPORT	b. ABSTRACT	c. THIS PAGE			Kurt Anderson
U	U	U	UU	40	19b. TELEPHONE NUMBER *(Include area code)* 518-276-6620

INSTRUCTIONS FOR COMPLETING SF 298

1. REPORT DATE. Full publication date, including day, month, if available. Must cite at least the year and be Year 2000 compliant, e.g. 30-06-1998; xx-06-1998; xx-xx-1998.

2. REPORT TYPE. State the type of report, such as final, technical, interim, memorandum, master's thesis, progress, quarterly, research, special, group study, etc.

3. DATE COVERED. Indicate the time during which the work was performed and the report was written, e.g., Jun 1997 - Jun 1998; 1-10 Jun 1996; May - Nov 1998; Nov 1998.

4. TITLE. Enter title and subtitle with volume number and part number, if applicable. On classified documents, enter the title classification in parentheses.

5a. CONTRACT NUMBER. Enter all contract numbers as they appear in the report, e.g. F33315-86-C-5169.

5b. GRANT NUMBER. Enter all grant numbers as they appear in the report. e.g. AFOSR-82-1234.

5c. PROGRAM ELEMENT NUMBER. Enter all program element numbers as they appear in the report, e.g. 61101A.

5e. TASK NUMBER. Enter all task numbers as they appear in the report, e.g. 05; RF0330201; T4112.

5f. WORK UNIT NUMBER. Enter all work unit numbers as they appear in the report, e.g. 001; AFAPL30480105.

6. AUTHOR(S). Enter name(s) of person(s) responsible for writing the report, performing the research, or credited with the content of the report. The form of entry is the last name, first name, middle initial, and additional qualifiers separated by commas, e.g. Smith, Richard, J, Jr.

7. PERFORMING ORGANIZATION NAME(S) AND ADDRESS(ES). Self-explanatory.

8. PERFORMING ORGANIZATION REPORT NUMBER. Enter all unique alphanumeric report numbers assigned by the performing organization, e.g. BRL-1234; AFWL-TR-85-4017-Vol-21-PT-2.

9. SPONSORING/MONITORING AGENCY NAME(S) AND ADDRESS(ES). Enter the name and address of the organization(s) financially responsible for and monitoring the work.

10. SPONSOR/MONITOR'S ACRONYM(S). Enter, if available, e.g. BRL, ARDEC, NADC.

11. SPONSOR/MONITOR'S REPORT NUMBER(S). Enter report number as assigned by the sponsoring/ monitoring agency, if available, e.g. BRL-TR-829; -215.

12. DISTRIBUTION/AVAILABILITY STATEMENT. Use agency-mandated availability statements to indicate the public availability or distribution limitations of the report. If additional limitations/ restrictions or special markings are indicated, follow agency authorization procedures, e.g. RD/FRD, PROPIN, ITAR, etc. Include copyright information.

13. SUPPLEMENTARY NOTES. Enter information not included elsewhere such as: prepared in cooperation with; translation of; report supersedes; old edition number, etc.

14. ABSTRACT. A brief (approximately 200 words) factual summary of the most significant information.

15. SUBJECT TERMS. Key words or phrases identifying major concepts in the report.

16. SECURITY CLASSIFICATION. Enter security classification in accordance with security classification regulations, e.g. U, C, S, etc. If this form contains classified information, stamp classification level on the top and bottom of this page.

17. LIMITATION OF ABSTRACT. This block must be completed to assign a distribution limitation to the abstract. Enter UU (Unclassified Unlimited) or SAR (Same as Report). An entry in this block is necessary if the abstract is to be limited.

FINAL PERFORMANCE REPORT

Abstract

At low Earth orbits (LEO), a differential in the drag acceleration between spacecraft can be used to control their relative motion. This differential allows for a propellant-free method for performing relative maneuvers, which can reduce the costs of spacecraft formations. In this project atmospheric differential drag (DD) based nonlinear controllers are presented that can be used for planar relative maneuvers of two spacecraft. The controllers were tested using high fidelity Systems Tool Kit (STK) simulations for re-phase, fly-around, and rendezvous maneuvers. Furthermore, the atmospheric density varies in time and in space as the spacecraft travel along their orbits. In this project a localized density predictor based on Neural Networks (NNs) was also developed. The predictor uses density measurements or estimates along the past orbits and can use a set of proxies for solar and geomagnetic activities to predict the value of the density along the future orbits of the spacecraft. The performance of the localized predictor is studied for different NN structures, testing periods of high and low solar and geomagnetic activity and different prediction windows. Comparison with previously developed methods show substantial benefits in using neural networks, both in prediction accuracy and in the potential for spacecraft onboard implementation.

List of symbols

a, b, c, d	Constants in Schweighart and Sedwick model
a_{Drel}	Magnitude of the aerodynamic drag acceleration experienced by spacecraft
a_{Dcrit}	Magnitude of the differential drag acceleration than ensures stability
$\mathbf{a}_{Prel}$	Differential accelerations caused by any additional perturbations
A_{bc}	Element of matrix $\underline{\boldsymbol{A}}_{\boldsymbol{d}}$ to which a_{Dcrit} is the most sensitive
$\underline{\boldsymbol{A}}_{\boldsymbol{d}}$	Stable linear reference state space matrix
$\underline{\boldsymbol{A}}_{\boldsymbol{s}}$	Schweighart and Sedwick model state space matrix
B	Spacecraft's ballistic coefficient, also bias in the context of the neural network predictors
C_D	Spacecraft drag coefficient
D	Number of delays in the hidden layer
Dst	Geomagnetic index
$\mathbf{e}$	Tracking error vector

$f(\cdot)$	Nonlinearities in the spacecraft dynamics, or nonlinearities in general in the context of Lyapunov stability, also nonlinear function in the context of the neural network predictors
$F_{10.7}$	Solar index
i_t	Target's initial orbit inclination
J_2	Second-order harmonic of Earth gravitational potential field (Earth flattening)
lb, up	Lower and upper bounds for the optimization
m	Spacecraft's mass
n	Mean motion
n_s	Number of samples in a data set
$\underline{\boldsymbol{P}}, \boldsymbol{P_v}$	Solution matrix of the Lyapunov equation and its vectorized form
$\underline{\boldsymbol{Q}}, \boldsymbol{Q_v}$	Selected Lyapunov equation matrix and its vectorized form
R_p	Pearson correlation coefficient
R_e	Earth mean radius
S	Spacecraft cross-wind section area for chaser and target spacecraft
t_s	Sampling period of the density data
T_1, T_2, T_3, T_4	Matrix transformations
u_d	Feedback linear control for reference system
$\hat{u}$	On-off control signal
$\underline{\mathbf{U}}_{nxn}, \underline{\mathbf{U}}_1, \underline{\mathbf{U}}_2$	Permutation matrices
V	Lyapunov function
W_p	Prediction window
$\mathbf{x_n}$	State space vector including relative position and velocity of the spacecraft system in the LVLH orbital frame
$\mathbf{x_d}$	Linear reference model state space vector in the LVLH orbital frame
ΔB	Ballistic coefficient differential
δ_A	Magnitude of the modification made to matrix $\underline{\boldsymbol{A}}_d$ using the switching adaptation
δ_{Aop}	Modifications made to matrix $\underline{\boldsymbol{A}}_d$ for the optimized adaptation
ι	Neural network input
μ	Gravitational parameter
o	Neural network output

ρ	Atmospheric density
$\hat{\rho}$	Predicted Atmospheric density
τ	Neural network target value

1. Introduction

Leonard et al. [1] introduced the concept of DD as an alternative method for generating the control forces required by the relative maneuvers on the orbital plane at LEO. The method consists of varying the aerodynamic drag experienced by different spacecraft, thus generating differential accelerations between them. The interest towards this methodology comes from the desire for efficient, autonomous spacecraft relative maneuvering. To increase the efficiency and economic viability of such maneuvers, propellant consumption must be reduced. Furthermore, since there is no propellant exhaust, sensitive onboard sensors will not be affected during maneuvers. However, maneuvering using DD requires the ability to generate magnitudes of differential acceleration larger than the accelerations caused by any other perturbations; hence, the spacecraft must be able to change their ballistic coefficients by the necessary amounts and their orbits must be low enough for providing enough drag force. Additionally, DD results in increased orbital decay.

Using DD for spacecraft relative maneuvering presents two main challenges. Firstly, motion on the orbital plane is to be controlled; therefore, two degrees of freedom, motion along the orbit and along the radial direction of the spacecraft, are to be controlled. Conversely, drag force acts only along the orbit of the spacecraft, and influences the motion along the radial direction through the coupling in the dynamics. Accordingly, the spacecraft system is under actuated when using DD for controlling its dynamics on the orbital plane. Secondly, the magnitude of the DD acceleration fluctuates during the maneuver as the spacecraft encounters regions of the thermosphere with varying atmospheric density. These variations are difficult to predict on board. This means that the control force (drag force) is difficult to know with certainty prior to the maneuver. This works presents methods specially developed for addressing these issues.

This work presents the development of novel nonlinear control strategies, based on the Lyapunov approach, to perform spacecraft relative maneuvers at LEO, exploiting atmospheric drag forces. Furthermore, a localized predictor based on NNs for the estimation of future values of the drag acceleration experienced by spacecraft along its orbit is also developed as complement for the Lyapunov controllers. The use of the predictor will provide the guidance and control systems with estimates of the available drag force along the future orbit of the spacecraft. Such tools will provide a framework from which autonomous propellant-less spacecraft relative maneuvering using atmospheric DD acceleration can be realized.

The problem of designing a control system for the maneuvering using DD becomes the problem of designing a real-time logic (i.e., the control action is computed as the maneuver progresses) to command the deployment or retraction of the drag surfaces, with the intent of forcing the satellites to follow a desired trajectory, a reference model or simply regulate to a desired final state. The sought-for logic needs

to be based on the assumption that the control is either positive maximum, negative maximum, or zero, neglecting the time required to deploy or retract the drag surfaces. In essence, a Lyapunov function of the tracking error is selected, and the control signal is chosen so that the tracking error converges to zero (i.e., the first order time derivative of the Lyapunov function is negative), thus, the nonlinear dynamics of the system (that is the real motion of the spacecraft) are forced to follow a desired trajectory, reference model or desired final state (regulation). This simplifies the control problem, since the desired trajectory can be designed using controlled linear dynamics approximating the reality of spacecraft relative motion. The controllers developed by the author build upon and improve work presented and tested in [2-4].

In order to enhance the performance of the Lyapunov controller, a way for adapting the Lyapunov function, in terms of the amount of drag acceleration necessary for stability, was developed. The definition of appropriate Lyapunov functions is a challenge that varies from problem to problem, and a widely studied theory exists (see [5-7]). In this work, a quadratic Lyapunov function of the tracking error is defined, and its positive definite matrix is changed using adaptations, effectively changing the Lyapunov function in real-time to improve controller performance (control effort and maneuver duration) during the maneuvers. Two adaptation strategies were developed, the switching adaptation and the optimized adaptation. The adaptations are achieved through analytical expressions giving the dependence of the critical value (minimum magnitude of the DD acceleration necessary to retain Lyapunov stability) on the chosen stable linear model. By means of these relationships, the amount of DD acceleration necessary to maintain stability is reduced while maneuvering, achieving a better control authority margin in real-time. Overall, the development of the adaptive Lyapunov controllers provides a valuable method that can be implemented onboard real spacecraft, even small spacecraft, with limited computing capabilities. In fact, the Lyapunov controllers require only onboard measurements (relative position and velocity) that would be available during flight.

To develop the density predictor, a similar approach to that of Stastny et al. [8] was used in this work. However, NNs are used instead of a linear model. NNs are capable of forecasting nonlinear behaviors since they contains nonlinearities in their neurons, and therefore it have the potential to accurately model the nonlinear behavior of the density along the orbit of the spacecraft. To train, validate, and test the NNs, density data from the CHAllenging Minisatellite Payload (CHAMP, see [9]) mission was used.

The main contributions of this projects to the state of the art are:

1) Analytical expressions for:
    a. A DD control law, which dictates the activation of the drag surfaces, based on Lyapunov principles (presented in [10]).
    b. The magnitude of the DD acceleration that ensures stability in the sense of Lyapunov for the system (critical value), presented in [11, 12]. Paper [11] was the winner of the best

student paper award for the category Spacecraft GNC at the 1st International Academy of Astronautics Conference on Dynamics and Control of Space Systems and was later published in the Acta Astronautica Journal as [12].

c. The partial derivatives of the critical value of the DD acceleration in terms of $\underline{\boldsymbol{Q}}$ (Lyapunov equation matrix), and $\underline{\boldsymbol{A}_d}$ (reference linear dynamics matrix). These derivatives were first introduced for the case of regulation only in [11, 12], and later generalized for tracking a trajectory or a reference model in [13, 14]. Matrices $\underline{\boldsymbol{Q}}$ and $\underline{\boldsymbol{A}_d}$ are independent variables that are chosen by the designer in the development of the Lyapunov control law.

2) Adaptation strategy, based on the partial derivative of the critical value in terms of matrix $\underline{\boldsymbol{A}_d}$, which chooses in real-time an appropriate positive definite matrix $\underline{\boldsymbol{P}}$ in a quadratic Lyapunov function, such that it reduces the critical value (presented by the author in [11, 12]).

3) A second adaptation strategy also based on the same partial derivative, which chooses an appropriate positive definite matrix $\underline{\boldsymbol{P}}$ in a quadratic Lyapunov function, such that it minimizes the critical value.

4) Demonstration of feasibility of the approach via numerical high fidelity orbital simulations using STK for three different maneuvers: a re-phase, a fly-around and a rendezvous

5) Development of neural network-based localized models, that are capable of forecasting the density to be encountered by a spacecraft along its orbit for prediction windows of one, eight and 32 orbits into the future (i.e. approximately 90min, 12hr and two days respectively), presented by the author in [15].

6) Appropriate design of the NN structure using different parameters such as the sampling rate of the data, the number of neurons in the hidden layer and the number of delays of the input.

7) Tests of the NN predictors over periods of high and low solar and geomagnetic activities.

8) Comparison of the results of the NN predictors with a simple persistence model, a linear model, JB2006, and HASDM (the latter three obtained from [8]) for the one-orbit forecast.

The following assumptions were made in the developments of this project:

- Two spacecraft (target and chaser) are considered, which have the ability of changing their ballistic coefficients by deploying or retracting a set of surfaces.
- The discussion in this work will be limited to in-plane motion, assuming that no out-of-plane is present, or that it is controlled with different means.
- The drag surface deployment/retraction time is assumed to be negligible with respect to the duration of the maneuvers. Thus, it is assumed the drag surfaces deploy/retract instantly, generating a bang-off-bang control profile, as suggested in [2, 3, 16 and 17,].

- The attitude is stabilized by other means than DD.

This document is organized as follows. Section 2 presents all the original developments in this project, including: the Lyapunov controller, the adaptive and adaptive optimized Lyapunov controllers, and the NN based predictors. Section 3 summarizes and comments the results of this work, including: the results from the STK simulations of the relative maneuvers using the controllers developed and the results of the tests done to the NN predictors. Finally, section 4 draws the conclusions.

2. Procedure

In this work the spacecraft relative motion is represented in the local vertical local horizontal (LVLH) reference frame. In this frame the origin of this frame orbits with the target spacecraft, x points from Earth to the target spacecraft (virtual or real), z points along the angular momentum vector of the target's orbit, and y completes the right-handed frame. The following equations were used for represent the relative motion dynamics for a chaser and target spacecraft in the LVLH frame:

$$\dot{\mathbf{x}}_{\mathrm{n}} = \begin{bmatrix} \underline{\mathbf{0}}_{2x2} & \underline{\mathbf{I}}_{2x2} \\ \underline{\mathbf{0}}_{2x2} & \underline{\mathbf{0}}_{2x2} \end{bmatrix} \mathbf{x}_{\mathrm{n}} + \begin{bmatrix} 0 \\ 0 \\ f_x(\mathbf{x}_{\mathrm{n}}) \\ f_y(\mathbf{x}_{\mathrm{n}}) \end{bmatrix} + \begin{bmatrix} 0 \\ 0 \\ 0 \\ a_{Drel} \end{bmatrix} = f(\mathbf{x}_{\mathrm{n}}) + \begin{bmatrix} 0 \\ 0 \\ 0 \\ a_{Drel} \end{bmatrix},$$

$$\ddot{x}_{\mathrm{n}} = f_x(\mathbf{x}_{\mathrm{n}}) = \mu\left(\frac{1}{R_t^{\,2}} - \frac{R_t + x_{\mathrm{n}}}{\left(\left(R_t + x_{\mathrm{n}}\right)^2 + y_{\mathrm{n}}^{\,2} \right)^{3/2}} \right) + 2\omega\dot{y}_{\mathrm{n}} + 2\omega^2 x_{\mathrm{n}} + a_{\mathrm{Pr}elx}, \tag{1}$$

$$\ddot{y}_{\mathrm{n}} = f_y(\mathbf{x}_{\mathrm{n}}) + a_{Drel} = -\mu\left(\frac{y_{\mathrm{n}}}{\left(\left(R_t + x_{\mathrm{n}}\right)^2 + y_{\mathrm{n}}^{\,2} \right)^{3/2}} \right) + 2(\omega^2 y_{\mathrm{n}} - \omega\dot{x}_{\mathrm{n}}) + a_{\mathrm{Pr}ely} + a_{Drel}$$

The magnitude of the relative acceleration caused by the differential aerodynamic drag for the spacecraft system (target and chaser) is given as:

$$a_{Drel} = \frac{1}{2}\rho\Delta B v_s^2 \tag{2}$$

where ΔB is the difference in ballistic coefficients between the target and chaser. The ballistic coefficient is defined as

$$B = \frac{C_D S}{m} \tag{3}$$

Furthermore, the Schweighart and Sedwick [18] linear model was used to create the reference model for the development of the controller. This model assumes that the target's orbit is circular, that the only perturbation acceleration is caused by the J_2 perturbation, and that the separation between spacecraft is small compared to the radii of their orbits. Schweighart and Sedwick model can be formulated as the following system:

$$\dot{\mathbf{x}}_l = \begin{bmatrix} \underline{\mathbf{0}}_{2x2} & \underline{\mathbf{I}}_{2x2} \\ \left(5c^2 - 2\right)n^2 & 0 \quad 0 \quad 2nc \\ 0 & 0 \quad -2nc \quad 0 \end{bmatrix} \mathbf{x}_l + \begin{bmatrix} 0 \\ 0 \\ 0 \\ a_{Drel} \end{bmatrix} = \underline{\mathbf{A}}_s \mathbf{x}_l + \begin{bmatrix} 0 \\ 0 \\ 0 \\ a_{Drel} \end{bmatrix} \tag{4}$$

$$c = \sqrt{1 + \frac{3J_2 R_e}{8R_t^{\,2}}[1 + 3cos(2i_t)]}, \qquad n = \frac{\omega}{c}$$

In essence the Lyapunov controller used in this work forces a nonlinear model to follow a stable linear reference system. A quadratic function of the tracking error (difference between the state of the nonlinear and the stable linear reference systems) is defined. Afterwards a control law aimed to satisfy the Lyapunov theorem as defined in [19]. The stable linear reference system can be tracking a desired guidance trajectory or can be regulated; furthermore the stable linear reference system can be replaced by a desired guidance trajectory or by a constant state vector.

$$\begin{aligned} V &= \boldsymbol{e}^T \underline{\boldsymbol{P}} \boldsymbol{e}, \quad \boldsymbol{e} = \mathbf{x}_{\mathrm{n}} - \mathbf{x}_d, \\ \dot{V} &= -\mathbf{e}^T \underline{\boldsymbol{Q}} \mathbf{e} + 2\left(\mathbf{e}^T \underline{\boldsymbol{P}} \boldsymbol{B} a_{Drel} \hat{u} - \mathbf{e}^T \underline{\boldsymbol{P}} \left(\underline{\boldsymbol{A}}_{\boldsymbol{d}} \mathbf{x} - \boldsymbol{f}\left(\mathbf{x}\right) + \boldsymbol{B} u_d\right)\right) \end{aligned} \tag{5}$$

where $\underline{\boldsymbol{P}}$ is a symmetric positive definite matrix and $\boldsymbol{e}$ is the tracking error vector, $\hat{u}$ is the command sent to the surface actuators, the matrix $\underline{\boldsymbol{Q}}$ is chosen such that a Lyapunov equation is satisfied ($\underline{\boldsymbol{A}}_{\boldsymbol{d}}^T \underline{\boldsymbol{P}} + \underline{\boldsymbol{P}} \underline{\boldsymbol{A}}_{\boldsymbol{d}} = -\underline{\boldsymbol{Q}}$), and the matrices $\underline{\boldsymbol{A}}_{\boldsymbol{d}}$ and $\boldsymbol{B}$ represent a stable linear reference dynamics (in this work the Schweighart and Sedwick stabilized using an LQR).

The resulting control law presented in [10] can be expressed as:

$$\hat{u} = -sign(\boldsymbol{e}^T \underline{\boldsymbol{P}} \underline{\boldsymbol{B}}) \tag{6}$$

It is worth emphasizing that all the components in this control law would be available in real-time onboard a spacecraft. For the actual implementation of the controller this activation strategy is applied every 10 minutes, to give the drag forces enough time to change the net accelerations of the spacecraft.

A critical value (a_{Dcrit}) of differential drag that is needed to maintain stable Lyapunov control was developed in [11, 12]. This critical value is given as:

$$a_{Dcrit} = \frac{\mathbf{e}^T \underline{\boldsymbol{P}} \left(\underline{\boldsymbol{A}}_{\boldsymbol{d}} \mathbf{x}_{\mathrm{n}} - \boldsymbol{f}\left(\mathbf{x}\right) + \boldsymbol{B} u_d\right)}{\left|\mathbf{e}^T \underline{\boldsymbol{P}} \boldsymbol{B}\right|} \tag{7}$$

The analytical expression for the partial derivative of the critical value with respect to the matrix $\underline{\boldsymbol{A}}_{\boldsymbol{d}}$ (in Equation (8)) was developed in [11, 12]. The matrix $\underline{\boldsymbol{A}}_{\boldsymbol{d}}$ is set by design, so it can be manipulated to reduce the value of the critical value during the maneuver, provided that it remains Hurwitz. The element of matrix $\underline{\boldsymbol{A}}_{\boldsymbol{d}}$, to which a_{Dcrit} is the most sensitive (A_{bc}, the entry with the largest partial derivative) is identified by calculating the partial derivative.

$$\begin{aligned} \frac{\partial a_{Dcrit}}{\partial \underline{\boldsymbol{A}}_{\boldsymbol{d}}} = {\mathrm{T}_3}^{-1}\left(\frac{\partial \underline{\boldsymbol{P}}}{\partial \underline{\boldsymbol{A}}_{\boldsymbol{d}}}\right)\left[\underline{\mathbf{I}}_{4x4} \otimes {\mathrm{T}_1}^{-1}\left(\frac{\partial \eta(\underline{\boldsymbol{P}})}{\partial \underline{\boldsymbol{P}}}\right)\right]\left[\underline{\mathbf{I}}_{4x4} \otimes \left(\underline{\boldsymbol{A}}_{\boldsymbol{d}} \mathbf{x} - \boldsymbol{f}\left(\mathbf{x}\right) + \boldsymbol{B} u_d\right)\right] + \\ \left[\underline{\mathbf{I}}_{4x4} \otimes \frac{\mathbf{e}^T \underline{\boldsymbol{P}}}{\left|\mathbf{e}^T \underline{\boldsymbol{P}} \boldsymbol{B}\right|}\right] \underline{\boldsymbol{U}}_{16x16} \left(\underline{\mathbf{I}}_{4x4} \otimes \mathbf{x}\right), \end{aligned} \tag{8}$$

For the details on the derivation of Equation (8) refer to [11, 12].

2.1 Adaptive and optimized adaptive Lyapunov controllers

To improve the performance of the Lyapunov controller an adaptation and an optimized adaptation of the drag surface activation strategy (Equation (6)) were developed. Both adaptations rely (a_{Dcrit}) and the partial derivative (Equations (7) and (8)).

2.1.1 Adaptation strategies

Changing the elements of matrix $\underline{\boldsymbol{A}}_d$ will change the critical value, which determines how much magnitude of the relative drag acceleration is needed to attain Lyapunov. Furthermore, modifying this matrix will also affect the control law via the matrix $\underline{\boldsymbol{P}}$ (see Equation (6)) thus changing how the Lyapunov controller reacts to the tracking error. This suggest that by changing this matrix the performance of the controller can be influenced. Two different adaptations were developed to enhance the performance of the Lyapunov controller taking advantage of this feature. These adaptations seek to reduce the critical value via modifications to matrix $\underline{\boldsymbol{A}}_d$ as the maneuver progresses. Both adaptations are implemented as illustrated in Figure 1. The adaptations are implemented such that the modified $\underline{\boldsymbol{A}}_d$ matrix is still stable and are applied at the same time as the activation strategy, which is every 10 minutes.

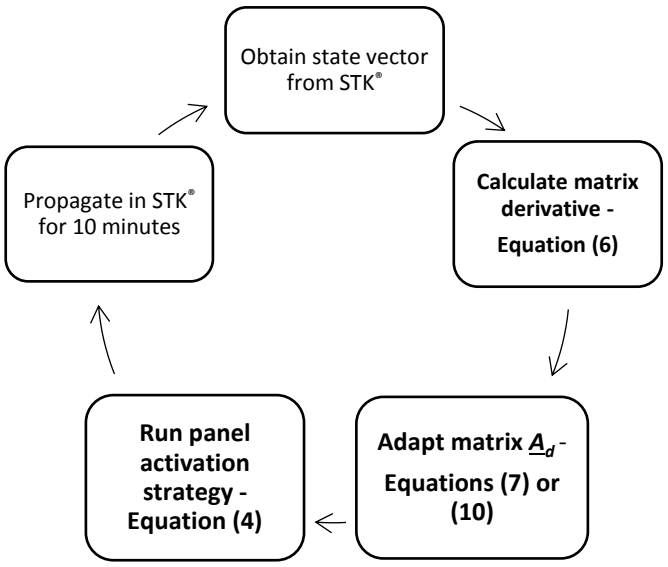

Figure 1. Control Strategy diagram, the text in bold represents the onboard control calculations, occurring every 10 minutes.

By calculating the partial derivative (Equation (8)) the entry of the matrix $\underline{\boldsymbol{A}}_d$, to which a_{Dcrit} is the most sensitive, is identified (that entry which has the partial derivative with the largest magnitude), which is defined as:

$$A_{bc} = A_{ij} \text{ for } \left|\frac{\partial a_{Dcrit}}{\partial A_{ij}}\right| > \left|\frac{\partial a_{Dcrit}}{\partial A_{kl}}\right| \text{ for } i, j \neq k, l \tag{9}$$

Once this entry is identified, it is switched to a small value (δ_A =10^{-6} which is in the same order of magnitude of the other entries of $\underline{\boldsymbol{A}}_d$). The sign of this modification is chosen such that it reduces the derivative of a_{Dcrit}, thus inducing a downward trend in the behavior of the critical value for the magnitude of the differential acceleration. By reducing this critical value, the overall robustness of the controller is improved since the control margin (the difference between the actual value of the DD acceleration and the critical value) is increased. The adaptive variations in $\underline{\boldsymbol{A}}_d$ are expressed as:

$$\frac{\Delta A_{ij}}{\Delta t} = \kappa_A \left[-sign\left(\frac{\partial a_{Dcrit}}{\partial A_{ij}}\right)\delta_A \right] \tag{10}$$

where κ_A is defined by:

$$\kappa_A = \begin{cases} 1 \text{ if } \left|\frac{\partial a_{Dcrit}}{\partial A_{ij}}\right| > \left|\frac{\partial a_{Dcrit}}{\partial A_{kl}}\right| \text{ for } i, j \neq k, l \\ 0 \text{ else} \end{cases} \tag{11}$$

The controller resulting from applying this adaptation to the Lyapunov control law developed in the previous section is called adaptive Lyapunov controller.

A further refinement of the adaptation strategy was achieved by including an optimization method, more specifically MATLAB's *fmincon* function, in the adaptation. The *fmincon* tool is an optimization method that finds the minimum of a constrained multivariate function.

For this adaptation the partial derivative defined in is again calculated and just as in the switching adaptation, the element of matrix $\underline{\boldsymbol{A}}_d$, to which a_{Dcrit} is the most sensitive (A_{bc}) is found. Afterwards, the *fmincon* function is used to minimize a_{Dcrit} in terms of A_{bc}. The optimization problem solved by *fmincon* can be formulated as:

$$\begin{aligned} \underset{A_{bc}}{\text{minimize}} \quad & a_{Dcrit}\left(A_{bc}\right) \\ \text{subject to} \quad & lb \le A_{bc} \le up \end{aligned} \tag{12}$$

where and *lb* and *up* are the lower and upper bounds for A_{bc}. These bounds were chosen to be -10^{-6} and 10^{-6} which are in the same order of magnitude of the other entries of $\underline{\boldsymbol{A}}_d$. The solution of the optimization problem gives the sign and magnitude (δ_{AOp}) with which A_{bc} is modified. The adaptive variations in $\underline{\boldsymbol{A}}_d$ are expressed as:

$$\frac{\Delta A_{ij}}{\Delta t} = \kappa_A \delta_{Aop} \tag{13}$$

where κ_A and is defined in Equation (11)

It should be noted that the adaptations occur every 10 minutes and that that for a bang-off-bang control the Δt from Equations (10) and (13) is essentially zero.

2.2 Density Predictors

The NN density predictor, developed in this work, uses density measurements or estimates on a given orbit and a set of proxies for solar and geomagnetic activities to predict the value of the density along the future orbit of the spacecraft.

2.2.1 Neural network used

A time-delay feed-forward Neural Network structure was chosen for the development of the density predictor. This NN architecture does not include any feedback loops, hence the feed-forward part of its name. This NN architecture contains a set of delays at the input layer that allow for retention of the evolution of the inputs in time, and enhances the ability of the network for forecasting applications. Furthermore, the NN predictor contains two layers (hidden or input layer, and output layer). The output layer contains one single linear neuron. The number of neurons and delays in the hidden layer were determined by testing different configurations. The results of these experiments are included in the results shown in section 3. A diagram of a time-delay feed-forward Neural Network is shown in Figure 2.

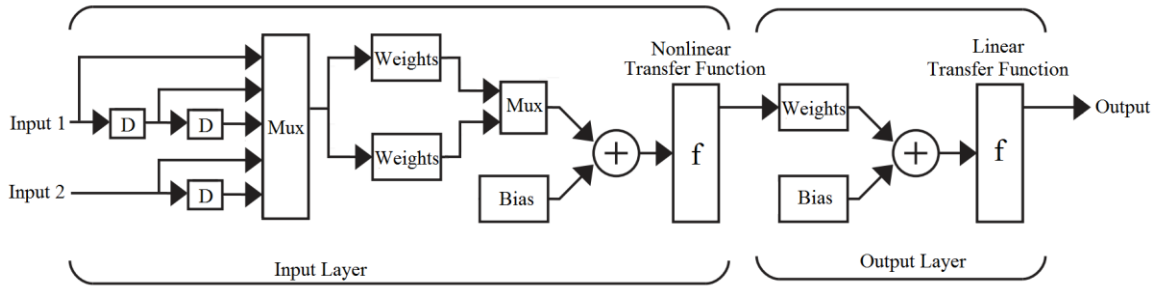

Figure 2. Diagram for a FTDNN with two layers, two inputs (one with two delays and the second one with one), two nonlinear neurons in the input layer and one linear neuron in the output layer.

In this application, the input to the NN is the present value of the density and the output is the predicted value over a predefined prediction window. Additional inputs such as the current values of the solar and geomagnetic indices (Dst and $F_{10.7}$) can also be included. The inputs are delayed a defined number of times inside the NN in order to capture some of their time evolution. Such formulation is shown in the following expression:

$$o\left(t+W_p\right)=f\begin{pmatrix}\iota\left(t-t_s\right),\ldots\iota\left(t-Dt_s\right),\\ DST\left(t-t_s\right),\ldots DST\left(t-Dt_s\right),\\ F_{10.7}\left(t-t_s\right),\ldots F_{10.7}\left(t-Dt_s\right)\end{pmatrix}, \qquad (14)$$

$$\iota=\ln\left(\rho\right),\qquad o=\ln(\hat{\rho})$$

where f is the overall nonlinear function of the neural network, ρ is the measured density, $\hat{\rho}$ is the predicted density value (from NN output), W_p is the prediction window, t_s is the sampling period of the data, t is the time, and D is the number of delays in the hidden layer.

The Levenberg-Marquardt algorithm (see [20, 21]) was used to train the NNs. This algorithm, which is included in MATLAB's Neural Network Toolbox ([22]), was chosen since it often has higher rates of convergence than the other algorithms provided in the Toolbox. The mean squared error (MSE), as explained in Equation (15), was selected as the performance function.

$$MSE = \frac{1}{n_s}\sum_{i=1}^{n_s}\left(o_i - \tau_i\right)^2 \tag{15}$$

where n_s is the number of samples, and τ is the target value

2.2.2 Density data used

The use of NNs requires data sets for training, validation, and testing the model's performance. The training and validation sets must contain data covering the different behaviors to be modeled by the neural network. CHAMP density data was used for this work. Measurements from the onboard accelerometer onboard the CHAMP satellite allow for the estimation of the density data. These data is available online and was obtained from [23].

For each NN the training density data was divided into two segments: one segment of past values, assumed to be available for the training and validation of the neural network; and one segment of future values, which are values of density that would not be available during training and validation, but instead are used exclusively for testing the NNs. The past values were sampled randomly and 70% were used for training, and the remaining 30% for validation. The available density data were not evenly distributed in time; therefore, for implementing the neural network, a linear interpolation was applied to make sure that there was a constant difference in time between consecutive samples in the data. The values of the density are in the order of magnitude of 10^{-12} kg/m^3 for day 140 of 2002. This results in numerical problems during the training of the NNs. To address this issue, the natural logarithm of the density values was used for the NNs instead of the density values themselves. Another advantage of using the natural logarithm, shown in [24], is that it often stabilizes the variance of the series, which allows for better modeling of the time series.

Several different periods of interest for training, validation, and testing the NNs were identified. Stastny et al. [8] chose two representative days for low and high geomagnetic activities for testing his linear model and for comparing it to JB2006 and HASDM. The first of these days was day 141 of 2002; during this day there was very low geomagnetic activity (Dst=-16, ap=10 and $F_{10.7}$=190.4). The second day used by Stastny et al. [8] was day 276 of 2001. During this day there was a moderate geomagnetic

storm, and as a result there was a higher geomagnetic activity (Dst =-107, ap=69 and $F_{10.7}$=191.8) For obtaining the linear model, Stastny et al. [8] used the data from day 140 (Dst =-12, ap=10 and $F_{10.7}$=175.4). This same data set was used to train, validate and test the NNs. These data sets included *n*=1080 data points for each day with a sampling rate of 80 sec.

To study the long-term performance of the NNs, it was decided to test them over one-year intervals. Out of the years that CHAMP was collecting data, years 2003 and 2007 were of special from the point of view of space weather and therefore were selected for testing. During 2003 (Dst =-22, ap=21.8 and $F_{10.7}$=128) the geomagnetic activity was the highest of that solar cycle (as explained in [25]). In contrast, during 2007 (Dst =-8, ap=7.5 and $F_{10.7}$=73) the solar cycle went through a period of very low activity (solar minimum, see [26]) and therefore the solar and geomagnetic activities were very low. The training and validation sets consisted of data from years previous to the testing years. Specifically, data from 2002 was used to train the NN for 2003 prediction, and data from 2006 was used to train the NN for 2007 prediction. For these long-term experiments a sampling rate of 120 sec was used. Figure 3 shows the daily averaged values for Dst, ap, and $F_{10.7}$ during 2003 and 2007.

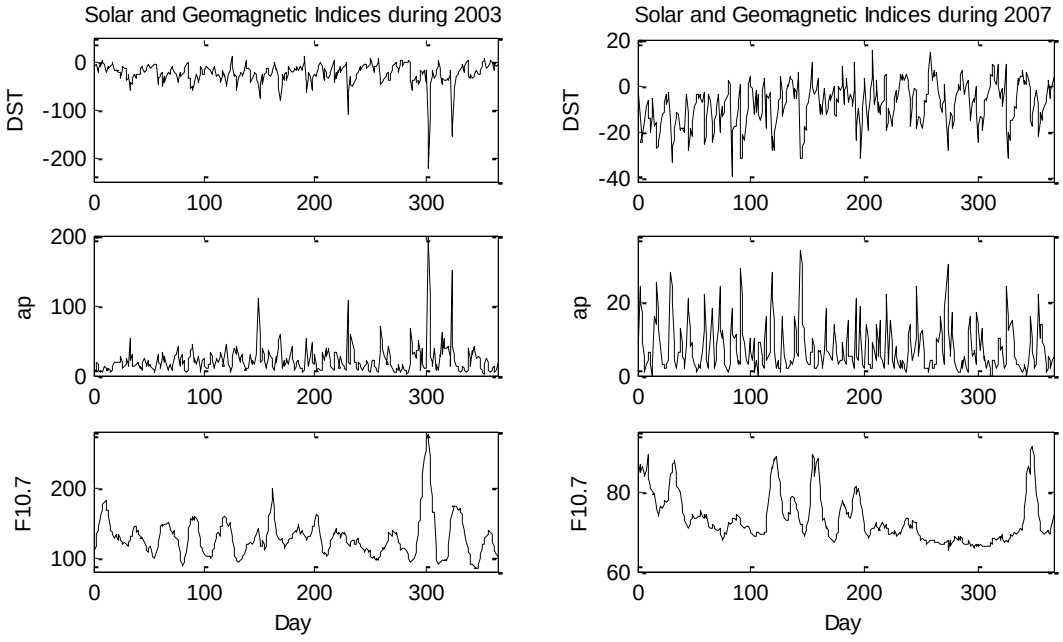

Figure 3. Dst, ap and F10.7 indices averaged daily for years 2003 (left) and 2007 (right).

2.2.3 Solar and geomagnetic indices

By including additional inputs other than the present density values, the performance of a NN as a predictor improves, provided that the output of the NN is a function of these inputs. Because the density is driven by the solar and geomagnetic activities, one proxy for each of these was selected as additional inputs. Out of the many possible choices (S_{10}, M_{10}, Mg II) $F_{10.7}$ was assumed to be a suitable proxy for the

solar activity affecting the density. This is a valid assumption since as pointed out by [27] there has not yet been any proof of one index been clearly superior to any other for satellite operations. Dst was assumed to be a valid proxy for geomagnetic activity. The ap index was not used since, as Figure 3 shows, Dst and ap are closely related. Furthermore as pointed out in [28], replacing ap for Dst reduced density errors especially during geomagnetic storms for Jacchia 70, NRLMSIS and JB 2008.

The indices were averaged hourly and were included in the corresponding training, validation, and testing sets. No interpolation was necessary for the indices since their sampling rate (hourly averaged values) was much larger than the sampling rate of the density (80 and 120 seconds) and there were no gaps in the data. For the one orbit prediction case at a sampling rate of 80 seconds, 68 samples per window are used; for the eight orbits case at a sampling rate of 120 seconds, 360 samples per window are used; and for the 32 orbits case at a sampling rate of 120 seconds, 1440 samples per window are used. As with the density values, during operation the NNs only have access to present values of the indices. The values for the Dst and $F_{10.7}$ indices used in this work were obtained from [29].

3. Numerical Results

3.1 Maneuver simulations

The three different Lyapunov controllers, developed in the previous section were tested and evaluated using numerical simulations. The guidance and control formulations have been programmed in MATLAB. These algorithms interact with STK via STK Connect. STK's High-Precision Orbit Propagator (HPOP) was used for modeling the mechanics of the maneuver, including J_2 perturbations, solar pressure radiation and variable atmospheric drag using the empirical NRLMSISE-00 model. The linear reference model and guidance trajectories are modeled using Simulink in the initialization part of the simulation (prior to running STK). The simulation architecture can be seen in Figure 4. For all of the simulations, the non-adaptive version (with constant $\underline{\boldsymbol{P}}$ and $\underline{\boldsymbol{A}}_d$) was compared with the adaptive and optimized adaptive Lyapunov controllers (with variable $\underline{\boldsymbol{P}}$ and $\underline{\boldsymbol{A}}_d$). For the re-phase and rendezvous maneuvers, the simulations were stopped when the spacecraft were within 10 m of the desired final state. For the fly-around maneuver the simulation was stopped after 2.5 orbital periods after the guidance reached the final equilibrium orbit.

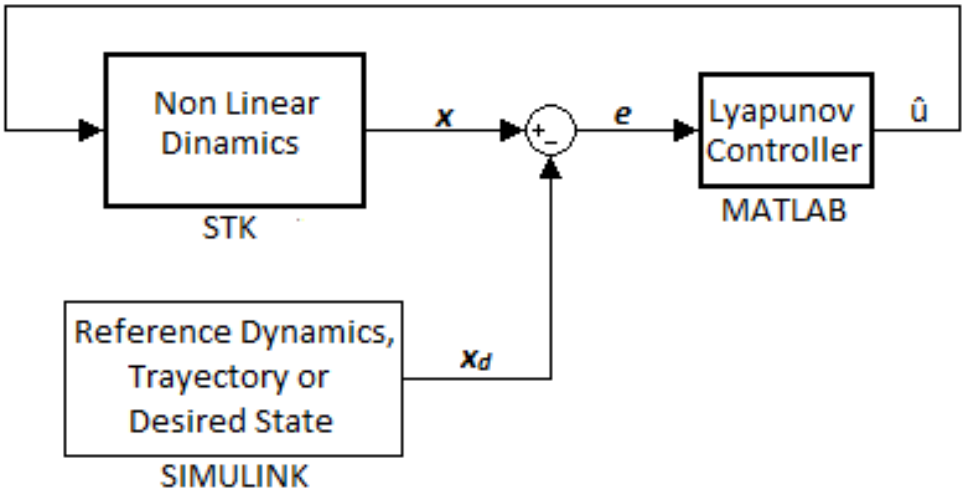

Figure 4. Simulation Diagram.

The three controllers can be implemented in the following configurations:

1) The controller forces the nonlinear system to go to a desired final state (regulation).

2) The controller is used to force the nonlinear system to directly track a generated guidance trajectory (no linear dynamics is defined).

3) The controller forces the nonlinear system to track the trajectory of the reference model which is tracking the generated guidance trajectory.

The initial orbital elements of the target (center of the LVLH frame) and other parameters for the numerical simulations are shown in Table 1. The target and chaser are assumed to be identical spacecraft, therefore they have the same ballistic coefficient and mass, for each surface configurations. The initial relative position and velocity of the chaser in the LVLH frame are shown in Table 2. For all simulations the initial $\underline{\boldsymbol{Q}}$ matrix was the identity matrix times 10^2.

Table 1. Spacecraft orbital Parameters and geometry.

Parameter	**Value**
Target's inclination (deg)	98
Target's semi-major axis (km)	6778
Target's right ascension of the ascending node (deg)	262
Target's argument of perigee (deg)	30
Target's true anomaly (deg)	25
Target's eccentricity	0
Maximum Ballistic Coefficient, surfaces deployed (m^2/kg)	0.625
Minimum Ballistic Coefficient, surfaces retracted (m^2/kg)	0.075
Mass (kg)	10

Table 2. Initial conditions in the LVLH frame.

Parameter	**Rendezvous**	**Fly-around**	**Re-phase**
x (km)	-1	0	0
y (km)	-2	-4.25	-1.9
$\dot{x}$ (km/sec)	4.8E-07	0	0
$\dot{y}$ (km/sec)	1.70E-04	0	0

These initial conditions where generated by selecting the orbits of the target and chaser and then calculating initial state vector (position and velocity of the chaser relative to the target).

3.1.1 Re-phase maneuver

For this simulation in STK, the initial difference in the *y* was -1.9km and the desired final difference was three km. The three controllers (Lyapunov, adaptive Lyapunov, and optimized adaptive Lyapunov controllers) were used in simulations for the re-phase maneuver. The controllers are used to regulate the error between the simulated relative positions and velocities and the desired final relative positions and velocities. For this maneuver the R_{LQR} value used to obtain the initial $\underline{\boldsymbol{A}}_d$ was 10^{18}. The trajectories in the LVLH are compared in Figure 5. Figure 6 shows the control signals for the three controllers. Tracking error plots are shown in Figure 7.

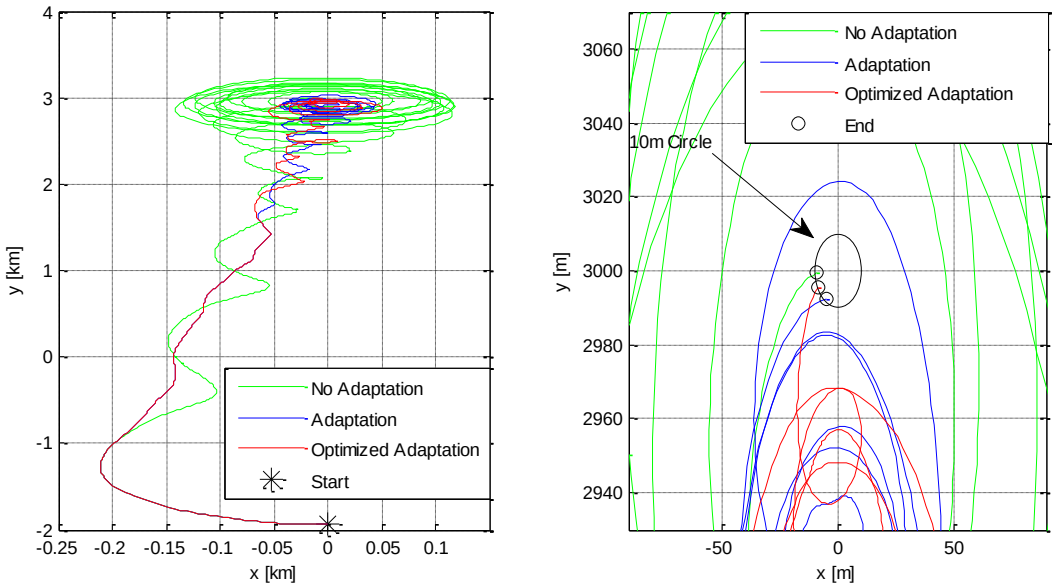

Figure 5. Re-phase maneuver trajectories in the x–y plane: (left) complete maneuver and (right) final stages of the maneuver.

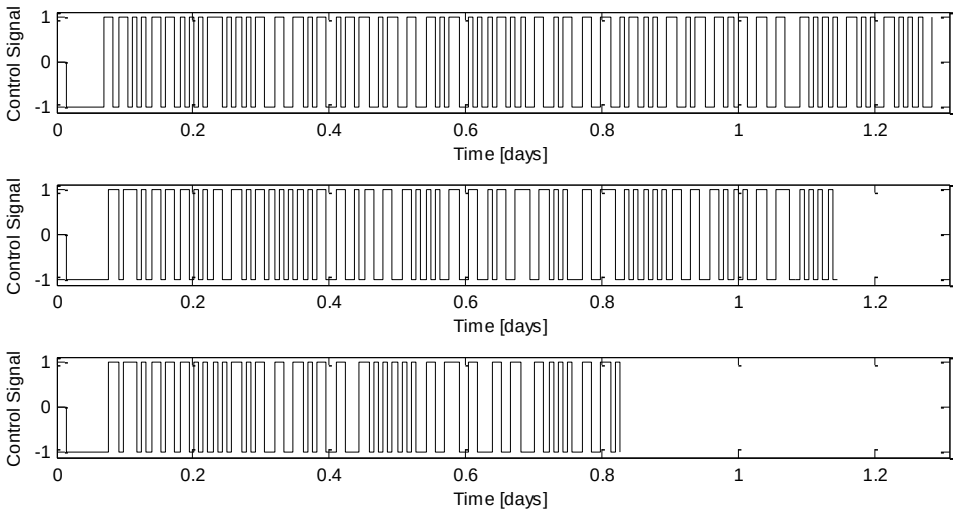

Figure 6. Re-phase maneuver control signals: (top) non-adaptive Lyapunov controller, (middle) adaptive Lyapunov controller and (bottom) adaptive optimized Lyapunov controller.

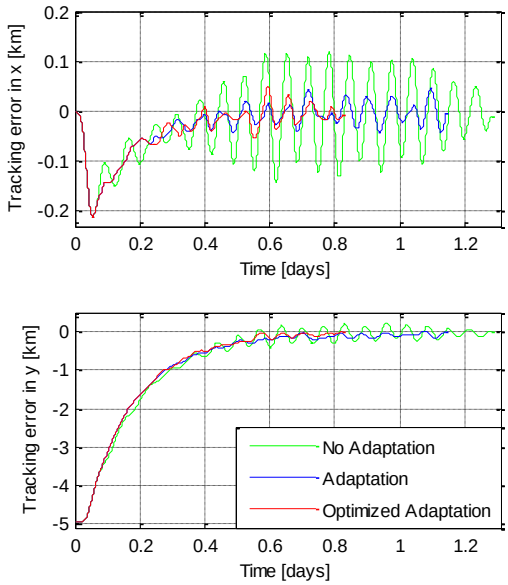

Figure 7. Tracking error over the entire re-phase maneuver: (top) x error and (bottom) y error.

3.1.2 Fly-around maneuver

Again the three controllers (Lyapunov, adaptive Lyapunov, and optimized adaptive Lyapunov controllers) have been used in simulations for the fly-around maneuver. In this case the controllers force the nonlinear dynamics to follow the desired fly-around guidance and not just to converge to a final state (second configuration). Moreover, the simulations are stopped 2.5 orbital periods after the guidance reaches the final equilibrium orbit. For this maneuver the R_{LQR} value was $1.6*10^{18}$. The guidance selected for the fly-around maneuver is based on Clohessy-Wiltshire equations and was obtained from [30]. The trajectories in the LVLH are compared in Figure 8, while Figure 9 shows the control signals for the three controllers. Tracking error plots are shown Figure 10.

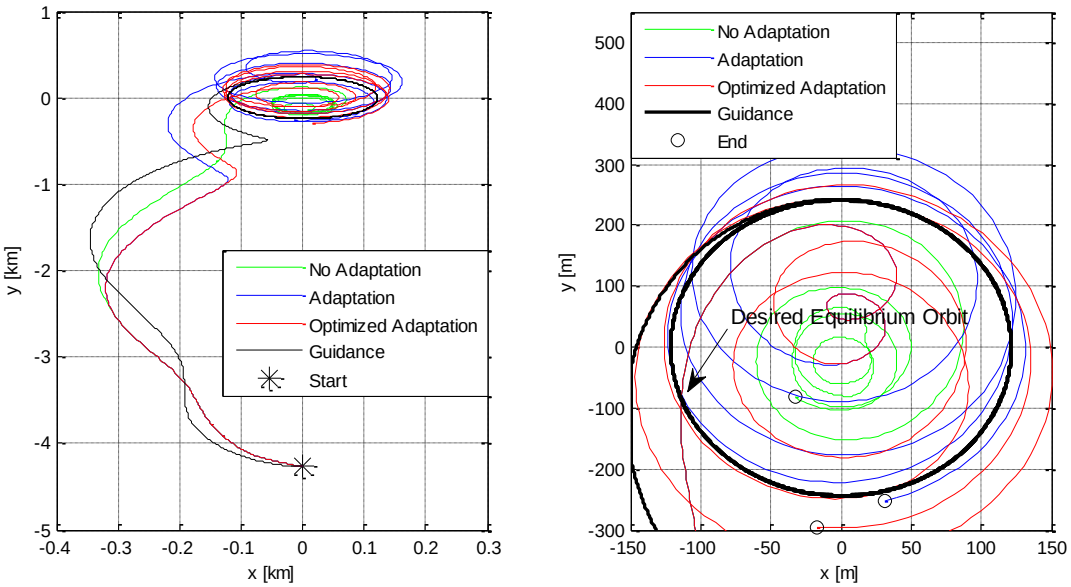

Figure 8. Fly-around trajectories in the x–y plane: (left) complete maneuver and (right) final stages of the maneuver.

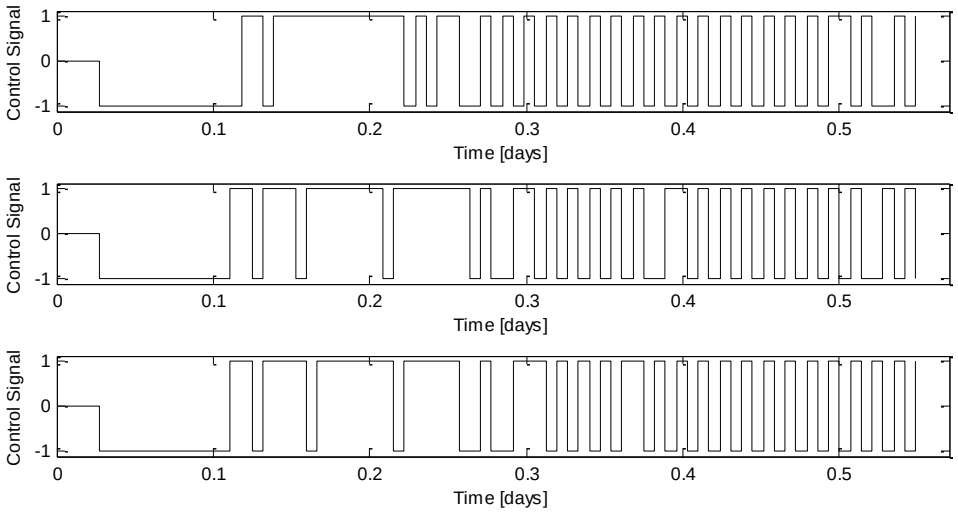

Figure 9. Fly-around maneuver control signals: (top) non-adaptive Lyapunov controller, (middle) adaptive Lyapunov controller and (bottom) adaptive optimized Lyapunov controller.

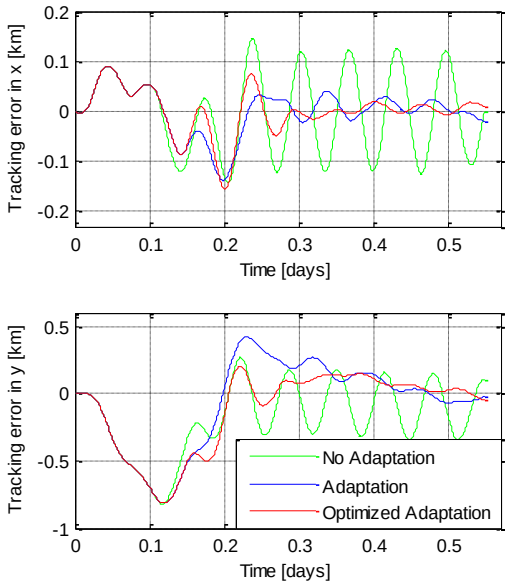

Figure 10. Tracking error over the entire fly-around maneuver: (top) x error and (bottom) y error.

3.1.3 Rendezvous maneuver

Of the three maneuvers simulated, the rendezvous maneuver is the most challenging using DD since it requires reducing an initial difference in the *x* direction as well as in the *y* direction. Since the system is underactuated, this requires introducing large errors in the *y* direction. For this maneuver the controllers have been implemented using the reference model tracking (third configuration).

A guidance trajectory based on Clohessy-Wiltshire equations has been selected for the rendezvous maneuvers. This guidance trajectory was made following the method described in [3] which uses a constant value for the density. In this simulation the controller forces the nonlinear system to track the trajectory of the reference model which is tracking the analytically generated guidance trajectory (third configuration). For this maneuver the R_{LQR} value was $1.6*10^{17}$. The trajectories in the LVLH are compared in Figures 11, 12 and 13. Figure 14 shows the control signals for the three controllers. Tracking error plots are shown Figure 15.

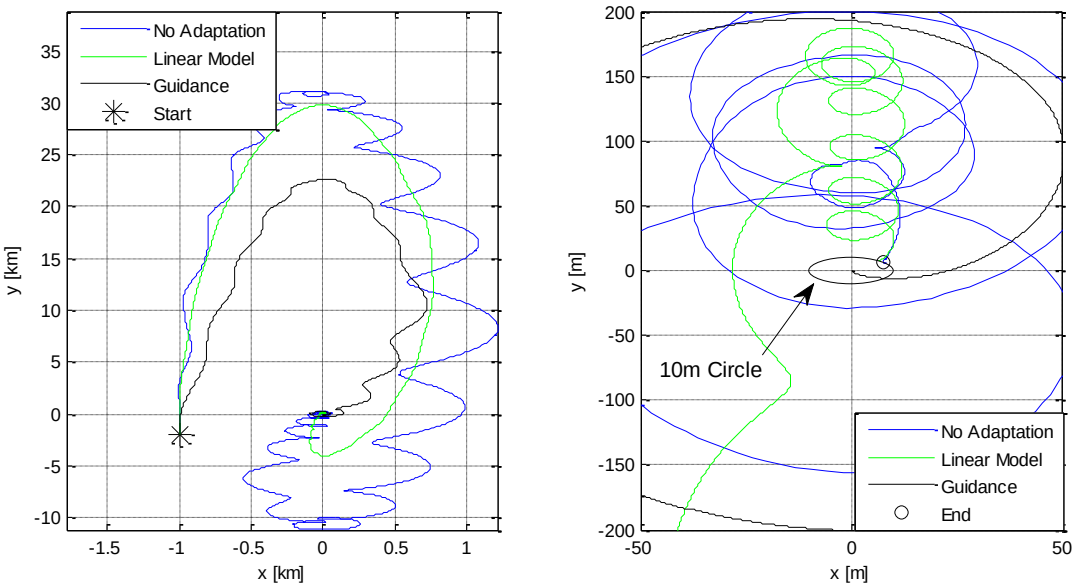

Figure 11. Rendezvous trajectories for the non-adaptive controller in the x–y plane: (left) complete maneuver and (right) final stages of the maneuver.

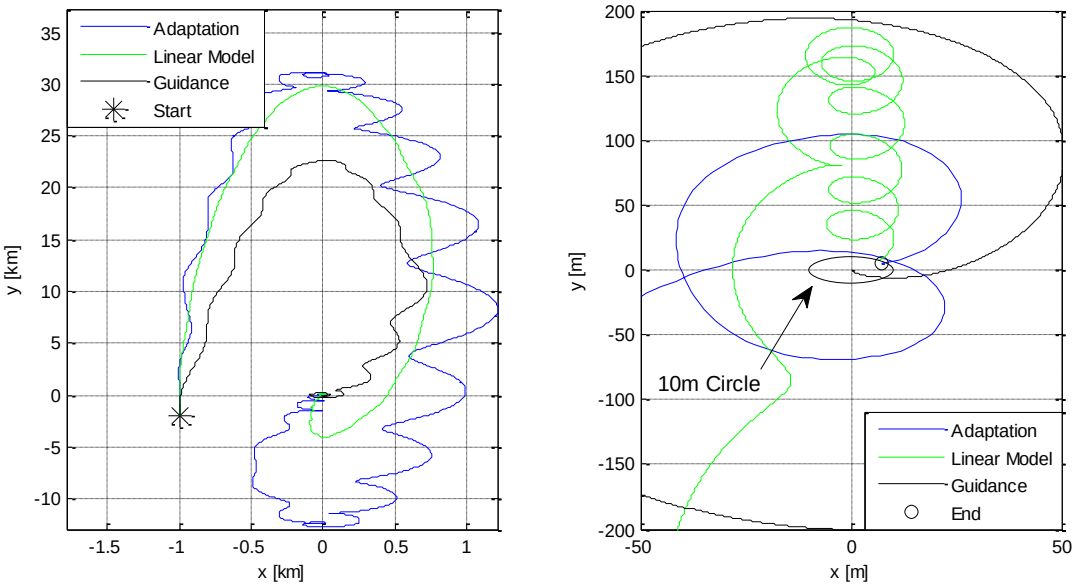

Figure 12. Rendezvous trajectories for the adaptive controller in the x–y plane: (left) complete maneuver and (right) final stages of the maneuver.

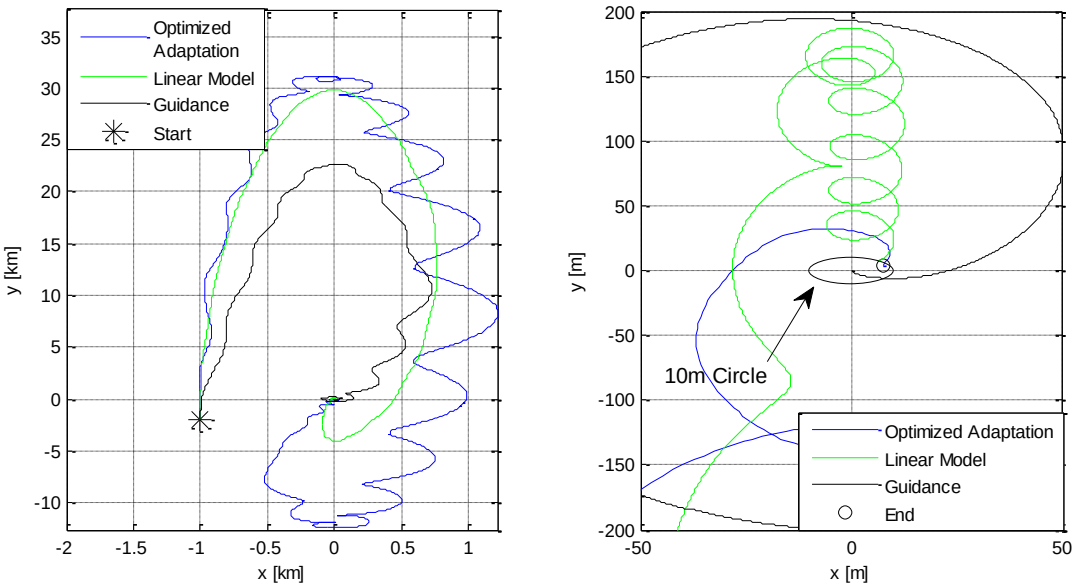

Figure 13. Rendezvous trajectories for the optimized adaptive controller in the x–y plane: (left) complete maneuver and (right) final stages of the maneuver.

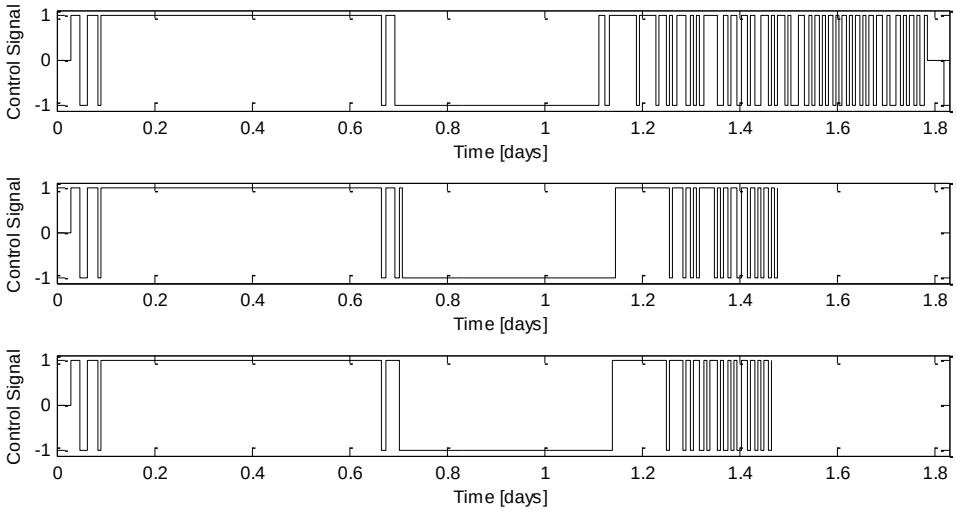

Figure 14. Rendezvous maneuver control signals: (top) non-adaptive Lyapunov controller, (middle) adaptive Lyapunov controller and (bottom) adaptive optimized Lyapunov controller.

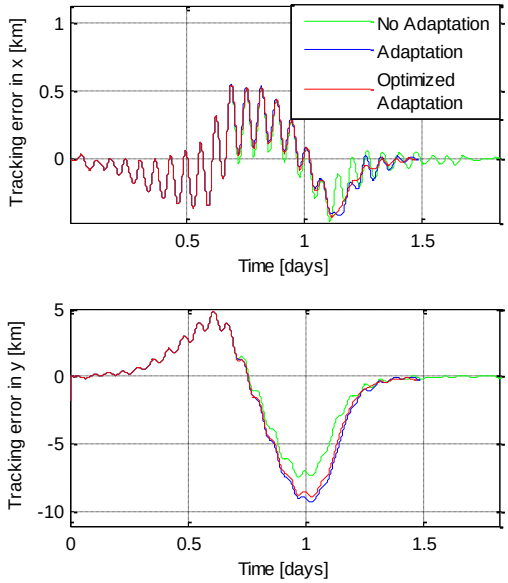

Figure 15. Tracking error over the entire rendezvous maneuver: (top) x error and (bottom) y error.

3.1.4 Controller performance assessment

The metrics used to evaluate the performance of the controllers are the number of switches in the control (control effort), the duration of the maneuver, the means for the critical and actual value of the DD acceleration, and the difference between these two values (control margin). The performance metrics for the simulations are shown in Table 3.

Table 3. Performance metrics for all maneuvers

Metric		Re-phase (Regulation)	Fly-around (Tracking Trajectory)	Rendezvous (Tracking Dynamics)
Non-Adaptive	Control changes	124	48	79
	Time (hr)	30.7	13.2	43.6
	Drag Mean Critical value (m/s^2)	-2.93E-07	-5.91E-06	-1.43E-04
	Mean Actual Drag(m/s^2)	9.61E-06	3.38E-05	3.42E-05
	Margin(m/s^2)	9.90E-06	3.97E-05	1.77E-04
Adaptive	Control changes	107	45	37
	Time (hr)	27.4	13.2	35.4
	Drag Mean Critical value (m/s^2)	-6.54E-07	-6.36E-06	-1.81E-04
	Mean Actual Drag(m/s^2)	9.52E-06	3.38E-05	3.49E-05
	Margin(m/s2)	1.02E-05	4.01E-05	2.16E-04
Optimized Adaptive	Control changes	73	46	35
	Time (hr)	19.8	13.2	35.1
	Drag Mean Critical value (m/s2)	-2.05E-06	-6.12E-06	-1.82E-04
	Mean Actual Drag(m/s2)	9.44E-06	3.38E-05	3.46E-05
	Margin(m/s2)	1.15E-05	3.99E-05	2.17E-04

As shown in Figures 5, 7, 11, 12, 13 and 15 for the re-phase and rendezvous maneuvers, all three controllers forced the chaser and target spacecraft to be within 10m of their desired final state. As seen in see Figure 8 for the fly-around maneuver the two adaptive controllers forced the system to reach an orbit close to the desired equilibrium final orbit (within ~50m); however, the non-adaptive reached an orbit with less precision than the other controllers (within ~300m). Furthermore, as can be observed in the tracking error plots (Figures 7, 10 and 15) both adaptive controllers produce smaller oscillations on the error, especially toward the end on the maneuvers, this produces smoother trajectories; even though, the control force is varying (since the density is varying).

The use of the adaptive controller reduced the control effort required to perform all three maneuvers with improvements relative to the non-adaptive of 13.7%, 6.3%, and 53.2% for the re-phase, fly-around and rendezvous maneuvers respectively. Similarly, the use of the optimized adaptive controller reduced

the control effort by 41.1%, 4.2%, and 55.7% in comparison with the non-adaptive for the re-phase, fly-around and rendezvous maneuvers respectively.

Likewise, the use of adaptive controller also reduced the duration of the maneuver with improvements of 10.9%, and 18.8% for the re-phase and rendezvous maneuvers respectively. Similarly, the use of the optimized adaptive controller reduced the duration of the maneuver with improvements of 35.7%, and 19.6% over the non-adaptive for the re-phase and rendezvous maneuvers respectively. There were no improvements in duration for the fly-around, since the simulations were not stopped when within 10m of the desired final position, but after 2.5 orbital periods after reaching the desired equilibrium relative orbit.

Furthermore, the adaptive controller also was able to increase the control margin by 2.9%, 1%, and 18.1% over the non-adaptive for the re-phase, fly-around, and rendezvous maneuvers respectively. Similarly, the optimized adaptive controller increased the control margin over the non-adaptive by 13.9%, 0.5%, and 18.4% over the non-adaptive for the re-phase, fly-around, and rendezvous maneuvers respectively.

Overall both adaptive and optimized adaptive controllers gave better results than the non-adaptive controller. The optimized adaptive gave better results than the adaptive for the re-phase (Regulation) and rendezvous (Tracking Dynamics) maneuvers; however, for the case of the fly-around (Tracking Trajectory), the performance metrics of the optimized adaptive were slightly worse than the adaptive. Nonetheless, Figure 10 shows that during the maneuver the errors were smaller for the optimized adaptive, so perhaps this came at a cost of higher slightly higher actuation (one more switch in the drag surfaces configuration).

3.2 Density Predictors

The training, validation, and testing of the NNs was done in MATLAB using the Neural Network Toolbox. As a benchmark for all the tests, a model using the persistence method was used. The persistence method is a very simple technique for forecasting in which the prediction is equal to the input. In other words, a predictor forecasting the density using the persistence method will predict the density in the future to be the same as it is in the present, so if the prediction window is one orbit, then each predicted orbit is equal to the previous measured orbit.

To assess the performance of the different models, different metrics were used: the MSE (shown in Equation (15)), the mean of the ratio between the target and the outputs, its standard deviation and the Pearson correlation coefficient of the targets to the model outputs ($\boldsymbol{R_p}$).

3.2.1 Different number of neurons, delays and sampling rates

Given the selected structure of the NN predictors, the appropriate number of neurons, delays in the hidden layer, and the data sampling rate for the localized density forecasting problem were found. This was accomplished empirically by trying different combinations. All the tests performed for this purpose were run on days 141 of 2002 and 276 of 2001, with the training and validation sets being day 140 of 2002. As mentioned before, these days cover high and low geomagnetic activity and were used also by Stastny et al. [8] to test his linear model. To find the appropriate number of neurons and delays in the hidden layer and the sampling rate the NN shown in Figure 16 was used.

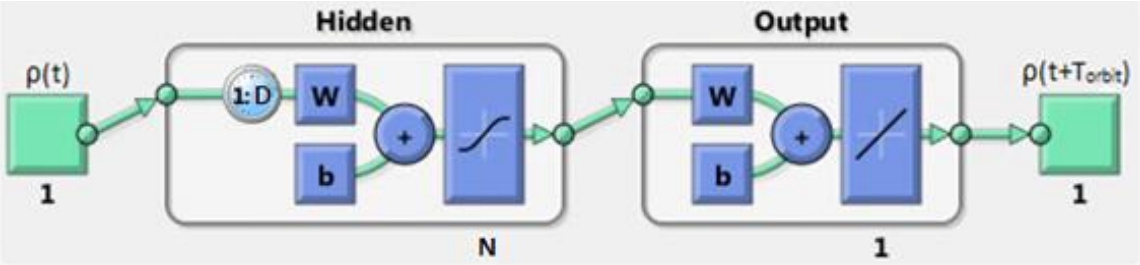

Figure 16. Neural network diagram where N and D are the numbers of neurons and delays in the hidden layer.

To find the appropriate number of neurons in the hidden layer several tests were performed in the sampling rate and the number of delays were fixed and the number of neurons was varied. Afterwards, the same procedure was followed for the number of delays and the sampling rate. The results for these tests are presented in [15]. The best results were obtained with one neuron in the hidden layer and enough delays to store from ¼ to one prediction window, while there was no significant difference in the performance when the sampling rate was below 180 seconds.

3.2.2 Predicting one orbit into the future on days 241 of 2002 and 276 of 2001

Once the appropriate structure of the NN was found several different NNs were tested again on days 141 of 2002 and 276 of 2001. This was done to evaluate the improvements in performance by increasing the size of the training and validation sets from one day to a year and also by using the solar and geomagnetic indices (Dst and $F_{10.7}$) as additional inputs. The one year training and validation data set used for testing the networks on day 141 of 2002 contained the data from the 365 preceding days (day 140 of 2001 to day 14 of 2002). The one year training and validation data set used for testing the networks on day 276 of 2001 contained the data from year 2002 (day 1 of 2002 to day 365 of 2002), since the CHAMP data did not went back a year before day 276 of 2001. Even though this means that the NN used was trained on data corresponding to the future of day 276 of 2001, the training data and validation data set is still different to the testing set which makes the test valid (of course for practical implementation of the NNs the training and validation set would always be past and therefore available values). A sampling

rate of 80 sec was used since it is the same used by Stastny et al. [8]. The results of the tests for days 141 of 2002 and 276 of 2001 are summarized in Table 4. As a benchmark the performance of a persistence model are also included. The persistence method is a very simple technique for forecasting in which the prediction is equal to the input.

Table 4. Results for predicting one orbit into the future.

Testing Data Set	**Model Configuration**	**MSE**	R_p	**Mean target/output**	**Stdev target/output**
Day 141 2002 CHAMP	NN, preceding 365 days for Training	0.0108	0.9843	0.9998	0.0039
	NN, preceding 365 days for Training, Dst and $F_{10.7}$	0.0108	0.9842	0.9998	0.0039
	NN, day 140 of data for Training	0.0156	0.9774	1.0008	0.0046
	Persistence Model	0.0234	0.9685	1.0003	0.0058
	Linear model*	N/A	N/A	1.0058	0.0822
	HASDM*	N/A	N/A	0.8662	0.1204
	JB2006*	N/A	N/A	0.8564	0.095
Day 276 2001 CHAMP	NN, year 2002 of data for Training	0.0229	0.9086	0.9999	0.0058
	NN, Year 2002 of data for Training, Dst and $F_{10.7}$	0.0225	0.9099	0.9999	0.0058
	NN, day 140 Year 2002 of data for Training	0.0229	0.9106	0.9995	0.0058
	Persistence Model	0.0328	0.8718	1.0001	0.007
	Linear model*	N/A	N/A	1.0094	0.0822
	HASDM*	N/A	N/A	0.8415	0.1344
	JB2006*	N/A	N/A	0.6471	0.1355

*Obtained from [8]

For the 2001 scenario, training data from 2002 is used, as Stastny et al. did in their work. Training with future values and "predicting" past values is valid from the point of view of neural network, since the training/validation and testing data sets are still different. The results in Table 4 indicate that the global models (HASDM and JB 2006 results obtained from Stastny et al. [8]) have large biases in their results for the test days. This causes their performance to be worse than the performance of all the other models including the persistence model. The NN predictors give significantly better results than the linear model from Stastny et al. [8]), the global models, and the persistence model. For day 141 of 2002, by increasing

the size of the training and validation sets, the performance of the NNs increases; however, for day 276 of 2001 there is not a significant improvement by increasing the size of the training and validation sets nor by including the solar and geomagnetic indices. The addition of the indices does not benefit the NNs because the number of delays (17 which corresponds to ¼ of the prediction window) cannot capture more than one value in time of the indices since, the indices are averaged hourly. This might be solved by increasing the number of delays. An alternative solution would be retaining the same number of delays, but space them non-uniformly in time.

For day 141 of 2002, using data from one year to train and validate the NN provided the best results. The actual output of this NN and the targets are shown in Figure 17 along with the prediction error. For day 276 of 2001, the NN that uses the additional inputs (Dst and $F_{10.7}$) and that was trained and validated using the data from one year yielded the best results. The actual output of this neural network, the targets, and the prediction error are shown in Figure 18.

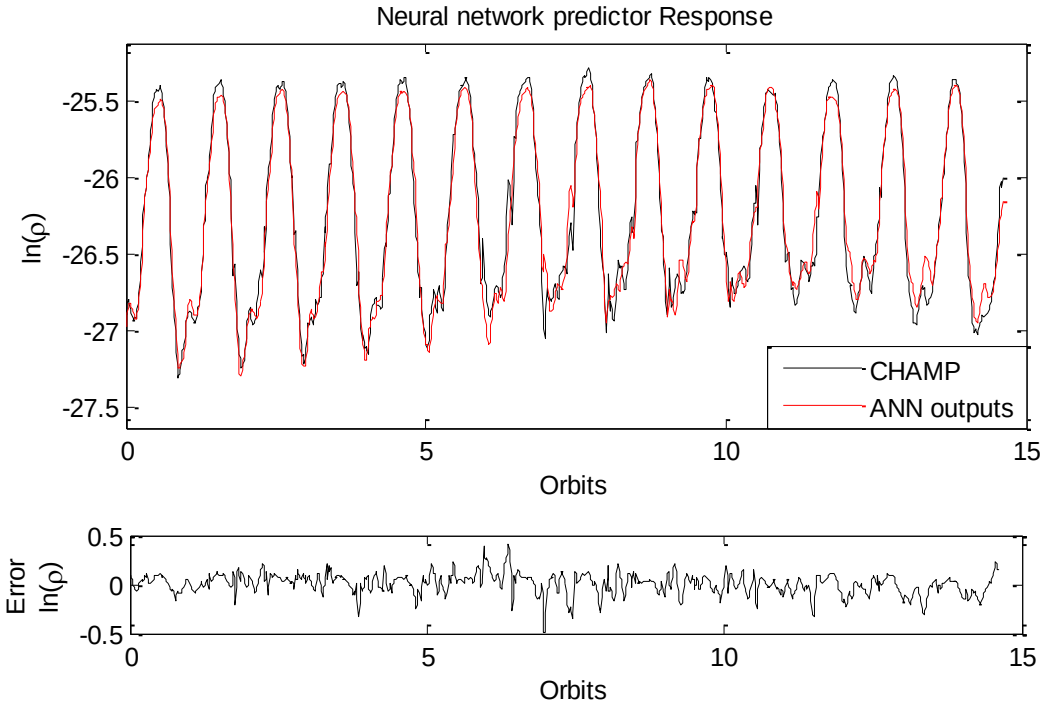

Figure 17. Neural network response for best case with a prediction window of one orbit over day 141 of 2002.

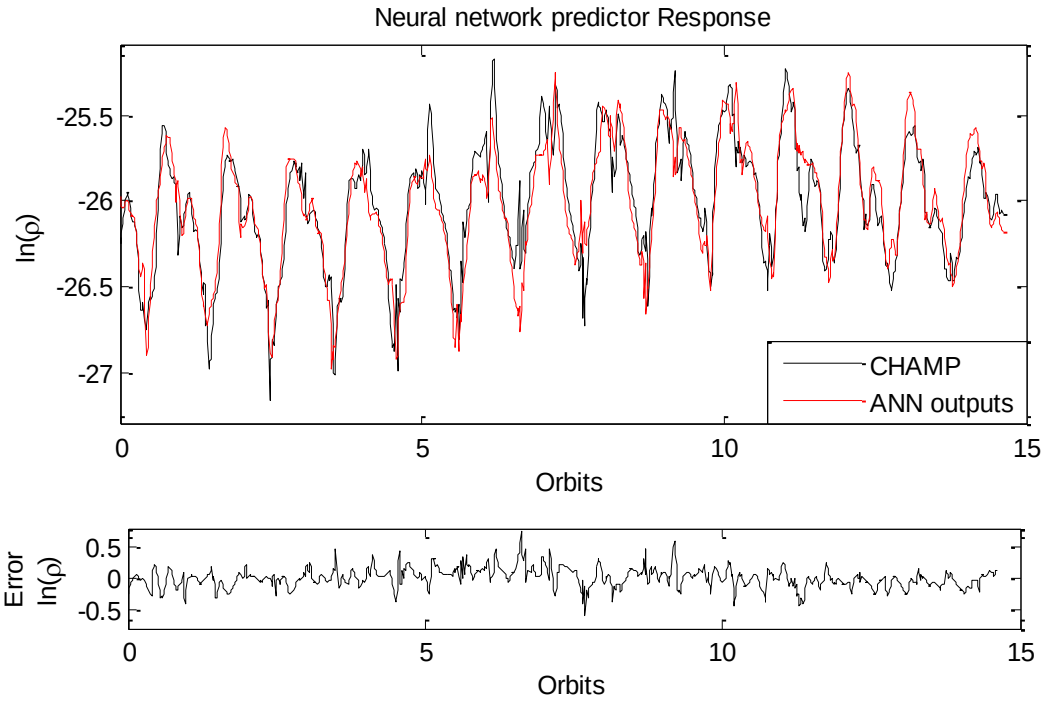

Figure 18. Neural network response for best case with a prediction window of one orbit over day 276 of 2001.

3.2.3 Predicting eight and 32 orbits into the future

For most applications of the NN density predictors, longer prediction windows are desired. For this reason additional NN predictors were trained, validated, and tested for predicting eight and 32 orbits into the future (approximately half a day and two days). For these results, the NNs were tested on years 2003 and 2007, in order to evaluate their performance over much wider data sets including periods of low and high solar and geomagnetic activities. As before, the use of additional inputs (Dst and $F_{10.7}$) was studied along with the use of different numbers of delays. Since having different sampling rates, as long as they are below 180 sec, does not affect significantly the NN performance, a sampling rate of 120 sec was used in order to reduce time for training and validation the NNs. The results are summarized in Tables 5 and 6 for the prediction windows of eight and 32 orbits respectively.

Table 5. Results for predicting eight orbits into the future.

Testing Data Set	Model Configuration	MSE	R_p	Mean target/output	Stdev target/output
CHAMP 2003	ANN, 90 delays (2 orbits), 1 year 2002 of data for Training	0.0433	0.8971	1.0007	0.0078
	ANN, 90 delays (2 orbits), 1 year 2002 of data and Dst and $F_{10.7}$ for Training	0.0429	0.8976	1	0.0078
	ANN, 360 delays (8 orbits), 1 year 2002 of data and Dst and $F_{10.7}$ for Training	0.0401	0.9044	0.9999	0.0075
	Persistence Model	0.2614	0.4037	1.0002	0.0192
CHAMP 2007	ANN, 90 delays (2 orbits), 1 year 2006 of data for Training	0.0417	0.9093	1.0002	0.0075
	ANN, 90 delays (2 orbits), 1 year 2006 of data and Dst and $F_{10.7}$ for Training	0.0407	0.9114	1	0.0074
	ANN, 360 delays (8 orbits), 1 year 2006 of data and Dst and $F_{10.7}$ for Training	0.0403	0.9122	1	0.0074
	Persistence Model	0.1902	0.6031	1.0001	0.016

The best case included in Table 5 for both years 2003 and 2007 were those obtained with the NN that included the additional inputs and that had 360 delays (one prediction window). Figures 19 and 20 show the MSE over the entire years 2003 and 2007 for the best cases along with the Dst and $F_{10.7}$ averaged daily.

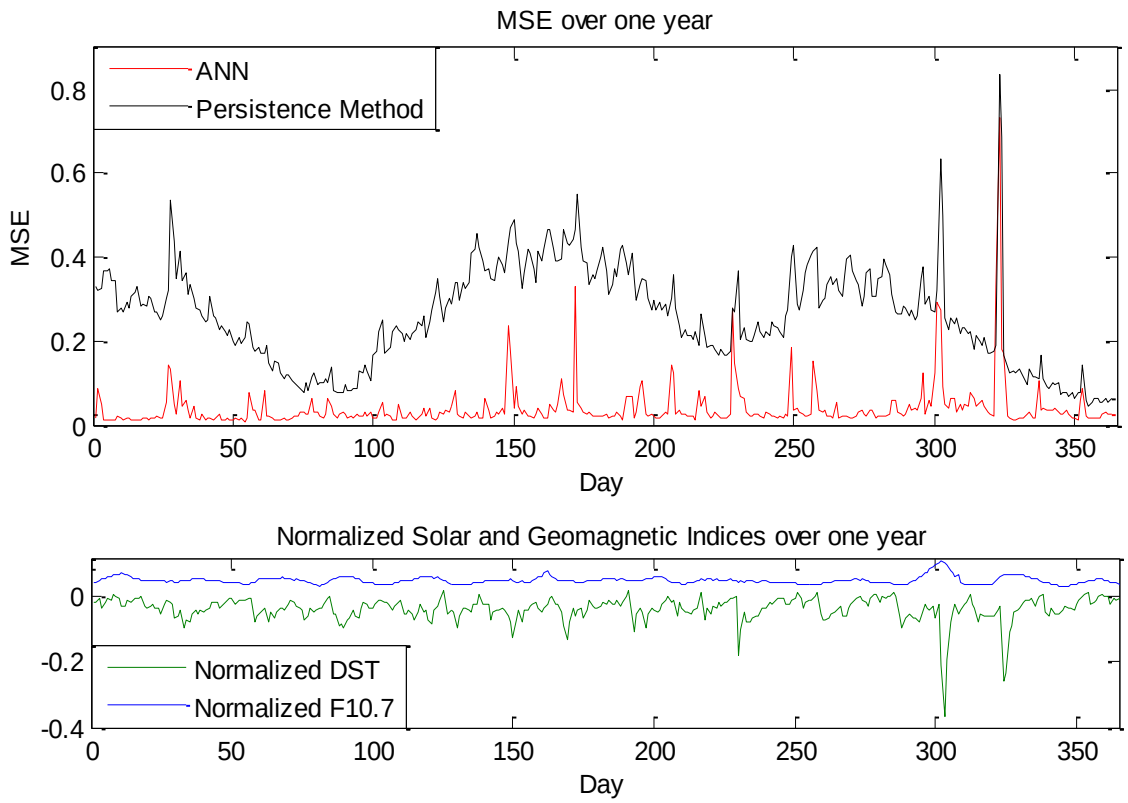

Figure 19. MSE for best case with a prediction window of eight orbits and normalized indices over year 2003.

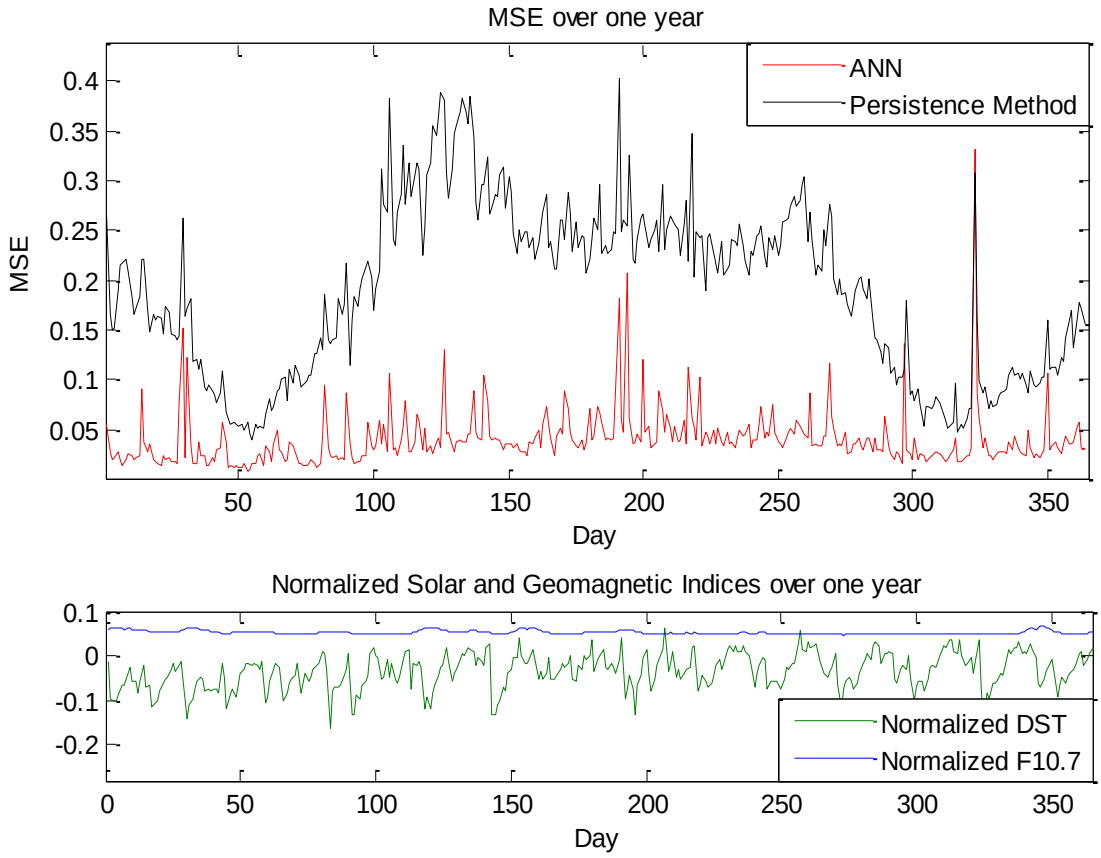

Figure 20. MSE for best case with a prediction window of eight orbits and normalized indices over year 2007.

Table 6. Results for predicting 32 orbits into the future.

Testing Data Set	Model Configuration	MSE	R_p	Mean target/output	Stdev target/output
CHAMP 2003	ANN, 360 delays (8 orbits), 1 year 2002 of data for Training	0.0917	0.7702	1.0013	0.0113
	ANN, 360 delays (8 orbits), 1 year 2002 of data and Dst and $F_{10.7}$ for Training	0.0895	0.774	1	0.0112
	Persistence Model	0.1813	0.5874	1.0001	0.016
CHAMP 2007	ANN, 360 delays (8 orbits), 1 year 2006 of data for Training	0.1564	0.6058	1.0009	0.0145
	ANN, 360 delays (8 orbits), 1 year 2006 of data and Dst and $F_{10.7}$ for Training	0.1515	0.6215	1.0002	0.0143
	Persistence Model	0.603	-0.2582	1.0005	0.0286

As indicated in Table 6 for the 32 orbit predictions the NNs yielded a better performance over the high activity period (2003) than the low activity one (2007). This was not observed in any of the other tests performed where the performance for both periods was almost the same or better for periods of low activity (see Tables 4 5). This indicates that for longer prediction windows over periods of low activity other unknown factors affect the density behavior, that are not well represented by the data used by the NNs (current value of the density, Dst and $F_{10.7}$ indices). This is here considered a topic for further investigation and beyond the scope of this work. Further investigation may lead to the discovery of unknown effects during periods of low activity.

The best case shown in Table 6 for both years 2003 and 2007 were those obtained with the NN that used the Dst and $F_{10.7}$ indices. The MSE over the entire years 2003 and 2007 for the best cases included in Table 6 (32 orbits prediction), along with the Dst and $F_{10.7}$ averaged daily are shown in Figures 21 and 22 for years 2003 and 2007 respectively.

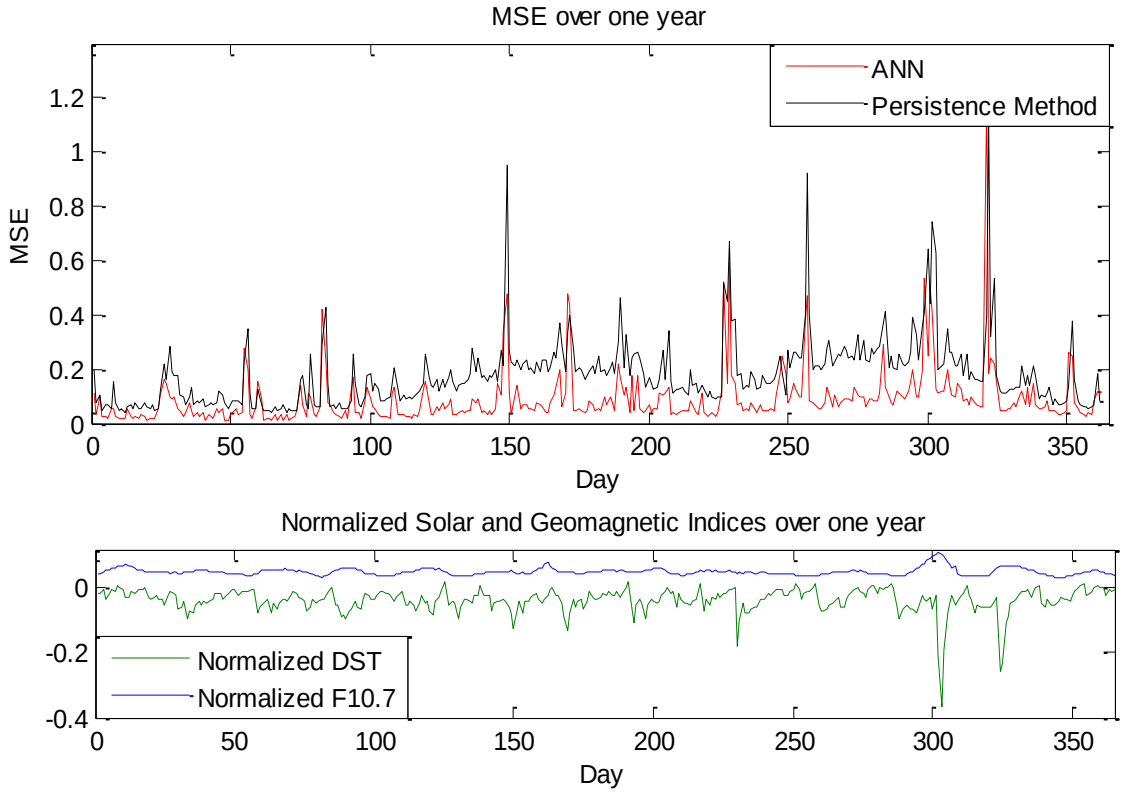

Figure 21. MSE for best case with a prediction window of 32 orbits and normalized indices over year 2003.

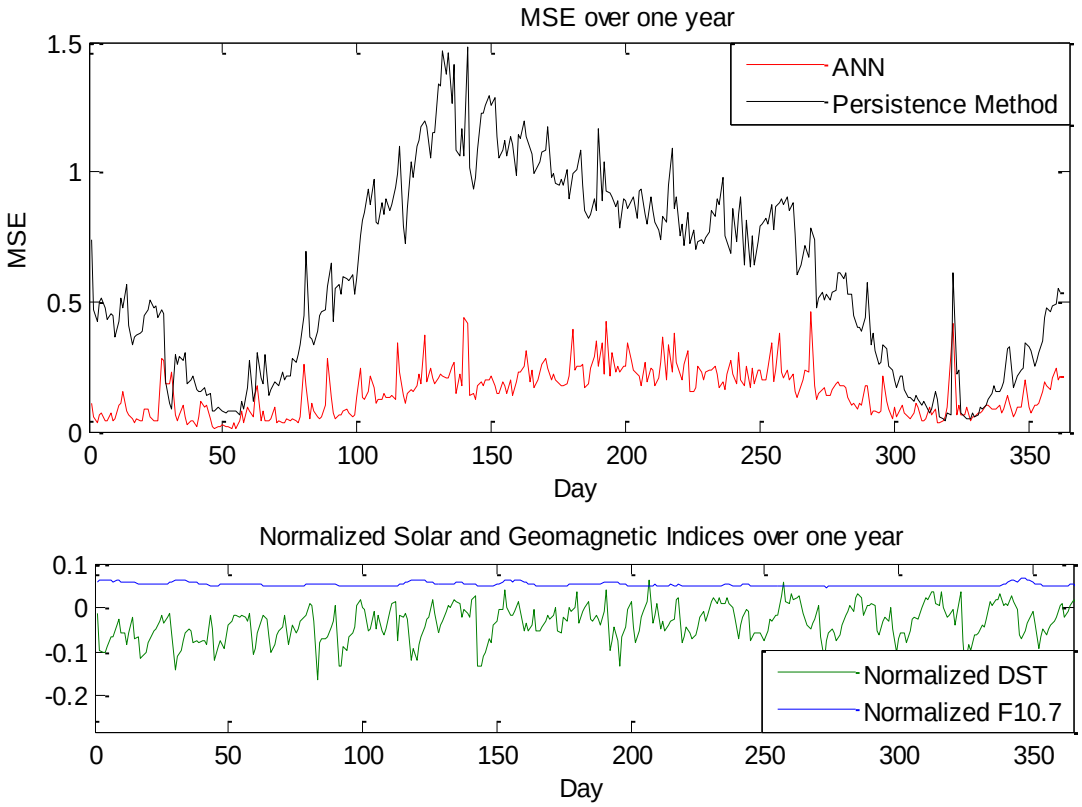

Figure 22. MSE for best case with a prediction window of 32 orbits and normalized indices over year 2007.

One very interesting feature can be observed in Figures 19 and 21. The peaks in the MSE correspond to peaks in the Dst index. This indicates that the NN predictors will have larger errors during geomagnetic storms. This is further confirmed by the results from the test performed for predicting one orbit into the future, in which the performance for the predictions on day 141 of 2002 were always better than the performance on day 276 of 2001, during which there was a geomagnetic storm.

From a computational point of view the training and validation of the NN predictors can be costly especially when dealing with large prediction windows (32 orbits into the future). For this reason, for future implementation of this work the training and validation processes are not recommended to be done onboard. Rather, it is proposed that density values obtained onboard via accelerometers be sent periodically to the mission team on the ground for training and validation. Once the weights and biases of the trained NN are obtained, they can be uplinked to the onboard computers and then the predictor can be used for onboard orbit propagation. The NN could then be re-trained on the ground as necessary.

4. Conclusions

This work developed methods for controlling the relative motion of a target and chaser spacecraft in the orbital plane using a differential in their drag accelerations, to enable propellant-less coplanar relative maneuvers in LEO. By varying the DD between the chaser, and target spacecraft their relative motion in the orbital plane is controlled. These variations are induced by changing the crosswind area of the spacecraft. The nature of this variation is assumed to be of bang-off-bang nature with only three possible values: maximum differential acceleration, minimum differential acceleration, and zero differential acceleration.

Lyapunov principles are used to develop a control law for the activation of the drag surfaces, thus allowing for any co-planar propellant-less spacecraft relative maneuvering, physically realizable with the small relative accelerations created by the difference in the drag forces acting on the spacecraft. The Lyapunov controller can be implemented by forcing the nonlinear dynamics to track a trajectory, the dynamics of a reference model, or to regulate to a desired final state. This allows for the implementation of the controller in maneuvers in which a specific path is desired, consequently, opening the possibilities for any other maneuver, provided that they are confined to the orbital plane and that they are realizable using the small acceleration created by the drag. The analytical nature of the methodology holds the promise for future onboard implementation on real spacecraft.

An analytical expression the magnitude of the DD that ensures stability (critical value) was developed. Analytical expressions for the partial derivatives of the DD critical value ensuring Lyapunov stability in terms of matrices $\underline{\boldsymbol{Q}}$ and $\underline{\boldsymbol{A}}_{\boldsymbol{d}}$ (chosen by the control designer, i.e., independent variables), were also developed. Two adaptations to the Lyapunov control law were developed. These adaptations use the partial derivative of the critical value in terms of matrix $\underline{\boldsymbol{A}}_{\boldsymbol{d}}$ to find the element of this matrix to which the critical value is the most sensitive. In the first adaptation, this element was changed by switching its value between fixed values to adapt the control law. In the second adaptation this element was changed to be the value that minimized (within a fixed range) the analytical expression of the critical value. The adaptations result in a matrix $\underline{\boldsymbol{A}}_{\boldsymbol{d}}$ that varies in time, and hence, so does the $\underline{\boldsymbol{P}}$ matrix in the quadratic Lyapunov function. Thus a new term, containing the time derivate of the $\underline{\boldsymbol{P}}$ matrix, appears in the Lyapunov function. An analytical expression for the time derivative of the $\underline{\boldsymbol{P}}$ matrix (assuming a continuous adaptation) was obtained in order to evaluate the impact of this new term in the stability of the system.

STK's HPOP was used to simulate the nonlinear dynamics of relative motion for spacecraft. In simulations the results for the re-phase, fly-around, and the rendezvous maneuvers indicate that the implementation of both the adaptive and optimized adaptive Lyapunov controllers allows for smoother maneuvers with less duration, less actuation, and greater control margin for the three different controller

configurations studied with respect to the non-adaptive controller. Furthermore, the optimized adaptive offers slightly better performance than the adaptive in terms of maneuver duration and control effort. The accuracy achieved with the proposed controllers is unprecedented for DD based relative maneuvering. For the rendezvous and re-phase maneuvers all controllers had the ability to take the spacecraft to within 10 meters of their desired final states, using only the differential in drag. Furthermore, for the fly around maneuver both adaptive controllers reached relative orbits very close to the desired final equilibrium relative orbit.

The NN predictors provided significantly better results than a linear model, and the global models HASDM and JB2006 for predicting the value of the density one orbit into the future for periods of high and low geomagnetic activity. The NN predictors were also tested for predicting eight and 32 orbits into the future (about half a day and two days at CHAMP's orbit). For these tests the performance of the NN predictors was evaluated over the years 2003 and 2007, which cover the periods with the high and low solar and geomagnetic activities. The performance of the NN predictors decreases as the prediction window increases, but even for the 32 orbit case, the results were satisfactory.

The NN predictors can also use the current value of the Dst (geomagnetic activity) and $F_{10.7}$ (solar activity) indices averaged hourly as additional inputs which resulted in an improvement of the performance of the NNs, provided that enough delays were included in the hidden layer to store some of the behavior in time of the indices. However, the number of delays cannot be increased beyond those required to store one prediction window or the NNs will suffer from overfitting in terms of the density values.

The controllers and the NN predictors are computationally simple and can be implemented onboard spacecraft. This would allow for accurate relative motion control using DD and precise onboard orbit propagation that can be used for navigation.

Acknowledgements

The contents of this report were published in [10-15, 31].

References

[1] Leonard, C. L., Hollister, W. M., and Bergmann, E. V., "Orbital Formationkeeping with Differential Drag," *AIAA Journal of Guidance, Control and Dynamics,* Vol. 12, No. 1, 1989, pp. 108–113. http://dx.doi.org/10.2514/3.20374

[2] Bevilacqua, R., and Romano, M., "Rendezvous Maneuvers of Multiple Spacecraft by Differential Drag under J_2 Perturbation," *AIAA Journal of Guidance, Control and Dynamics*, Vol. 31, No. 6, 2008, pp. 1595-1607. http://dx.doi.org/10.2514/1.36362

[3] Bevilacqua, R., Hall, J., S., and Romano, M., "Multiple Spacecraft Assembly Maneuvers by Differential Drag and Low Thrust Engines," *Celestial Mechanics and Dynamical Astronomy*, 2010, pp. 69–88. http://dx.doi.org/10.1007/s10569-009-9240-3

[4] Curti, F., Romano, M., and Bevilacqua, R., "Lyapunov-Based Thrusters' Selection for Spacecraft Control: Analysis and Experimentation," *AIAA Journal of Guidance, Control and Dynamics*, Vol. 33, No. 4, 2010, pp. 1143-1160. http://dx.doi.org/10.2514/1.47296

[5] Kamenetskiy, V. A., and Pyatnitskiy, Y. S., "A Gradient Method for Developing Lyapunov Functions in Problems of Absolute Stability," *Avtomatika i Telemekhanika*, No. 1, 1987, pp. 3-12.

[6] Kamenetskiy, V. A., and Pyatnitskiy, Y. S., "An iterative method of Lyapunov function construction for differential inclusions," *Systems & Control Letters*, Vol. 8, No. 5, 1987, pp. 445-451. http://dx.doi.org/10.1016/0167-6911(87)90085-5

[7] Barbashin, E. A., "On Construction of Lyapunov Functions for Nonlinear Systems," *Proceedings of the 1st Congress of the IFAC,* Moscow, USSR, June 1961, pp. 742-751.

[8] Stastny, N. B., Chavez, F. R., Lin, C., Lovell, A. T., Bettinger, R. A., and Luck, J., "Localized Density/Drag Prediction for Improved Onboard Orbit Propagation," *Proceedings of the Advanced Maui Optical and Space Surveillance Technologies Conference*, Curran Associates, Maui, HI, September 2009, pp. 51-58.

[9] Reigber, C., Lühr, H., and Schwintzer, P., "CHAMP Mission Status," *Advances in Space Research*, Vol. 30, No. 2, 2002, pp. 129–134. http://dx.doi.org/10.1016/S0273-1177(02)00276-4

[10] Pérez, D., and Bevilacqua, R., "Lyapunov-Based Spacecraft Rendezvous Maneuvers Using Differential Drag," *Proceedings of the AIAA Guidance, Dynamics and Control Conference 2011*, AIAA, Portland, OR, August 2011, pp. 7231-7253. http://dx.doi.org/10.2514/6.2011-6630

[11] Pérez, D., and Bevilacqua, R., "Differential Drag Spacecraft Rendezvous Using an Adaptive Lyapunov Control Strategy," *Proceedings of the 1st International Academy of Astronautics Conference on Dynamics and Control of Space Systems*, Univelt, Porto, Portugal, March 2012, pp. 973-991. http://dx.doi.org/10.1016/j.actaastro.2012.09.005

[12] Pérez, D., and Bevilacqua, R., "Differential Drag Spacecraft Rendezvous Using an Adaptive Lyapunov Control Strategy," *Acta Astronautica*, Vol. 83, 2013, pp. 196–207. http://dx.doi.org/10.1016/j.actaastro.2012.09.005

[13] Pérez, D., and Bevilacqua, R., "Spacecraft Maneuvering via Atmospheric Differential Drag Using an Adaptive Lyapunov Controller," *Proceedings of the 23rd AAS/AIAA Spaceflight Mechanics Meeting*, AIAA, Kauai, HI, February 2013, pp. 1-20.

[14] Pérez, D., and Bevilacqua, R., "Lyapunov-based Adaptive Feedback for Spacecraft Planar Relative Maneuvering via Differential Drag," *AIAA Journal of Guidance, Control, and Dynamics*, vol. 37, No. 5 ,2014, pp. 1678-1684. http://dx.doi.org/10.2514/1.G000191

[15] Pérez, D., Wohlberg, B., Lovell, T., Shoemaker, M., and Bevilacqua, R., "Orbit-Centered Atmospheric density prediction using artificial neural networks," *Acta Astronautica*, Vol. 98, 2014, pp. 9-23. http://dx.doi.org/10.1016/j.actaastro.2014.01.007

[16] Kumar, B., Ng, A., Yoshihara, K., and De Ruiter, A., "Differential Drag as a Means of Spacecraft Formation Control," *Proceedings of the 2007 IEEE Aerospace Conference*, IEEE, Big Sky, MT, March 2007, pp. 1-9. http://dx.doi.org/10.1109/aero.2007.352790

[17] Kumar, B. S., and Ng, A., "A Bang-Bang Control Approach to Maneuver Spacecraft in a Formation with Differential Drag," *Proceedings of the AIAA Guidance, Navigation and Control Conference and Exhibit*, AIAA, Honolulu, HI, August 2008, pp. 18-21. http://dx.doi.org/10.2514/6.2008-6469

[18] Schweighart, S. A., and Sedwick, R. J., "High-Fidelity Linearized J_2 Model for Satellite Formation Flight," *Journal of Guidance, Control, and Dynamics*, Vol. 25, No. 6, 2002, pp. 1073–1080. http://dx.doi.org/10.2514/2.4986

[19] Khalil, H. K., *Nonlinear systems*, 3rd ed., Prentice Hall, Upper Saddle River, NJ, 2002, Chap. 4.

[20] Levenberg, K., "A Method for the Solution of Certain Problems in Least Squares," *Quarterly of applied mathematics*, Vol. 2, 1944, pp. 164-168.

[21] Marquardt, D., "An Algorithm for Least-Squares Estimation of Nonlinear Parameters," *Journal of the Society for Industrial & Applied Mathematics*, Vol. 11, 1963, pp. 431-441. http://dx.doi.org/10.1137/0111030

[22] The MathWorks, "Levenberg-Marquardt backpropagation," *Documentation center* [commercial website], URL: http://www.mathworks.com/help/nnet/ref/trainlm.html [cited September 4, 2013].

[23] Forbes, J. M., Nerem, R. S, Sutton, E. K, Zhang, X., and Bruinsma, S., "Thermosphere Studies Using Accelerometer Measurements from the CHAMP and GRACE Satellites," *Department of Aerospace Engineering Sciences University of Colorado* [online database], URL: http://sisko.colorado.edu/sutton/ [cited August 19, 2013].

[24] Lütkepohl, H., and Xu, F., "The role of the log transformation in forecasting economic variables," *Empirical Economics, Springer*, Vol. 42, No. 3, 2012, pp. 619-638. http://dx.doi.org/10.1007/s00181-010-0440-1

[25] Belov, A. V., Gaidash, S. P., Ivanov, K. G., and Kanonidi, Kh. D., "Unusually High Geomagnetic Activity in 2003," *Cosmic Research*, Vol. 42, No. 6, 2004, pp. 541-550. http://dx.doi.org/10.1007/s10604-005-0001-0

[26] Belov, A. V., and Gaidash, S. P., "Anomalously low solar and geomagnetic activities in 2007," *Geomagnetism and Aeronomy*, Vol. 49, No. 5, 2009, pp. 566–573. http://dx.doi.org/10.1134/S001679320905003X

[27] Vallado, D. A., and Finkleman, D., "A Critical Assessment of Satellite Drag and Atmospheric Density Modeling*," Proceedings of the AIAA/AAS Astrodynamics Specialist Conference and Exhibit*, AIAA, Honolulu, HI, August 2008, pp. 18-21. http://dx.doi.org/10.2514/6.2008-6442

[28] Bowman, B. R., Tobiska, W. K., Marcos, F. A., Huang, C. Y., Lin, C. S., and Burke, W.J., "A New Empirical Thermospheric Density Model JB2008 Using New Solar and Geomagnetic Indices," *Proceedings of the AIAA/AAS Astrodynamics Specialist Conference*, AIAA, Honolulu, HI, August 2008b, pp. 1-19. http://dx.doi.org/10.2514/6.2008-6438

[29] Papitashvili, N., "OMNIWeb," *Goddard Space Flight Center Space Physics Data Facility* [online database], URL: http://omniweb.gsfc.nasa.gov/ow.html [cited August 19, 2013].

[30] Bevilacqua, R., "Analytical Guidance Solutions for Spacecraft Re-Phasing Based on Input Shaping," *AIAA Journal of Guidance, Control, and Navigation*, Vol. 37, No. 3, 2014, pp. 1042-1047. http://dx.doi.org/10.2514/1.G000008

[31] Pérez, D., "Adaptive Lyapunov control and artificial neural networks for spacecraft relative maneuvering using atmospheric differential drag," *Ph.D. Dissertation*, Mechanical, Aerospace, and Nuclear Engineering Dept., Rensselaer Polytechnic Institute., Troy, NY, USA, 2013.